NASA Technical Paper 3093

May 1991

Improvements in Computational Accuracy of BRYNTRN (A Baryon Transport Code)

Judy L. Shinn,
John W. Wilson,
Mark Weyland,
and Francis A. Cucinotta

NASA

NASA Technical Paper 3093

1991

Improvements in Computational Accuracy of BRYNTRN (A Baryon Transport Code)

Judy L. Shinn
and John W. Wilson
Langley Research Center
Hampton, Virginia

Mark Weyland
Kelsey-Seybold Clinic
Johnson Space Center
Houston, Texas

Francis A. Cucinotta
Rockwell International
Houston, Texas

National Aeronautics and Space Administration
Office of Management
Scientific and Technical Information Division

Abstract

The extension of the baryon transport code (BRYNTRN) for use in space radiation dose analyses for very large shield thicknesses is made possible by improving the numerical algorithms. The efforts were concentrated in obtaining more accurate, yet efficient, interpolation and integration methods at each local computational step, and in optimizing the grid distributions. A brief discussion of the nucleon transport theory and propagating formula is also given in conjunction with the analysis of error propagation which reveals the need for minimizing the local truncation errors. Sample calculations were made to verify the new algorithms. An accuracy of approximately 5 percent for a shield thickness of 150 g/cm^2 was found when a minimal 30-point energy grid was used. This accuracy was far superior to the results obtained by using the old algorithms where the solutions could be an order of magnitude different when a reasonably large number of grid points were used. The propagating step size was chosen such that the perturbation theory error matched the improved numerical accuracy.

Introduction

The recently developed, coupled neutron-proton baryon transport computer code (BRYNTRN) (ref. 1) using a deterministic approach for solving space radiation transport problems has been shown to be a convenient tool for the analysis of a shielding requirement against space protons for the future NASA manned space missions (refs. 2 and 3). The code has been used mostly to predict doses received by the astronauts inside a spacecraft of certain nominal thicknesses or in a storm shelter of a practically achievable quantity of mass. The accuracy of such analyses conducted by employing BRYNTRN can be assessed by the recent study (ref. 4) in which BRYNTRN and Monte Carlo calculations with shield thicknesses up to 30 g/cm^2 were compared and found to be within 10 percent.

The propagated error for a space-marching code such as BRYNTRN can become overwhelmingly large when the required number of computational steps increases. With the step size restricted to ensure that the perturbation series (ref. 5) will converge, BRYNTRN with existing numerical algorithms has been found to be quite satisfactory in marching through a thickness of 30 g/cm^2 or so. However, there are some applications that require the number of marching steps to increase enormously. For example, predicting the dose received by an astronaut in a very slender body like the Space Shuttle requires radiation transport calculations through rays up to 150 g/cm^2. Also, predicting radiation hazards for the passengers on a commercial subsonic high-altitude aircraft involves a radiation transport through the Earth's atmosphere of at least 200–300 g/cm^2 (refs. 6 and 7). In such cases, the number of marching steps becomes so large that the propagated (accumulated) error can distort the results or even destabilize the computation.

The present study places efforts on minimizing the local numerical errors of the existing BRYNTRN so as to reduce the propagated error and allow the code to be extended for use in space radiation application where the shield thickness is very large. The numerical algorithms will be improved to minimize the error but not to compromise the efficiency of the code. The computational step size will be examined and its maximum will be established so that the error from the perturbation technique will watch the improved accuracy of the new code. Sample calculations will be made to validate the new algorithms. A brief discussion is also given of the BRYNTRN nucleon transport method, the space-marching technique, and the propagation of errors.

Nucleon Transport Method

Since the protons produced by the solar particle events are energetic, the straight-ahead approximation is applied to the Boltzmann transport equations. The proposed perturbation theory (ref. 5) and the subsequently developed numerical technique (ref. 8) for solving the one-dimensional charged-particle transport equation

have been extended (ref. 9) to the coupled neutron-proton transport equations in BRYNTRN. In the following discussion, a one-dimensional charged-particle transport problem will be considered first for the purpose of presenting the numerical procedures and error analyses, and the final forms of propagating (space-marching) algorithms for the coupled neutron-proton transport equations will be given.

Charged-Particle Transport

The Boltzmann equation for proton transport in the straight-ahead approximation is given as

$$\left[\frac{\partial}{\partial x} - \frac{\partial}{\partial E}S(E) + \sigma\right] \phi(x,\, E) = \int_E^\infty f(E, E')\ \phi(x, E')\ dE' \tag{1}$$

where $S(E)$ is the proton stopping power as a function of energy E, σ is the macroscopic interaction cross section which we presently take as energy independent, $\phi(x, E)$ is the nucleon fluence spectrum at distance x, and $f(E, E')$ is the production secondary-particle spectrum by the primary particle of energy E'. Using the definitions

$$r = \int_0^E dE'/S(E') \tag{2}$$

$$\psi(x, r) = S(E)\ \phi(x,\, E) \tag{3}$$

and

$$\bar{f}(r, r') = S(E)\ f(E, E') \tag{4}$$

allows equation (1) to be written as

$$\left(\frac{\partial}{\partial x} - \frac{\partial}{\partial r} + \sigma\right) \psi(x, r) = \int_r^\infty \bar{f}(r, r')\ \psi(x, r')\ dr' \tag{5}$$

The advantage of equation (5) over equation (1) is that derivatives of $\phi(x, E)$ with respect to E display large variations at low energy and are difficult to approximate numerically, whereas $\psi(x, r)$ is well-behaved at all r values and approaches a constant at small values of r. The differential operator of equation (5) may be inverted to yield

$$\psi(x, r) = e^{-\sigma x}\ \psi(0,\, r{+}x) + \int_0^x dz\ e^{-\sigma z} \int_{r+z}^\infty dr'\ \bar{f}(r{+}z,\, r')\ \psi(x{-}z,\, r') \tag{6}$$

where the boundary condition is

$$\psi(0, r) = S(E)\ \phi(0, E) \tag{7}$$

A propagating algorithm for equation (6) is found by noting that

$$\psi(x{+}h,\, r) = e^{-\sigma h}\ \psi(x,\, r{+}h) + \int_0^h dz\ e^{-\sigma z} \int_r^\infty dr'\ \bar{f}(r{+}z, r'{+}z)\ \psi(x{+}h{-}z, r'{+}z) \tag{8}$$

which can be simplified by using

$$\psi(x{+}h{-}z, r) \approx e^{-\sigma(h-z)}\ \psi(x, r{+}h - z) + O(h) \tag{9}$$

which yields

$$\psi(x{+}h, r) \approx e^{-\sigma h}\ \psi(x, r{+}h) + e^{-\sigma h} \int_0^h dz \int_r^\infty dr'\ \bar{f}(r{+}z, r'{+}z)\ \psi(x, r'{+}h) \tag{10}$$

with the order of h^2, where h is the step size. Equation (10) is accurate for distances such that $\sigma h \ll 1$ and may be used to relate the spectrum at some point x to the spectrum at $x + h$. Therefore, one may begin at the boundary ($x = 0$) and propagate the solution to any arbitrary interior point using equation (10).

The secondary-source spectra $\bar{f}(r, r')$ in the integral portion of equation (8) are of the form

$$\bar{f}(r, r') \approx a e^{-\alpha r} + c e^{\gamma(r - r')} \tag{11}$$

where the coefficients α and γ are slowly varying functions of r', c is related to the quasielastic cross section, and a is determined by the normalization

$$\int_0^{r'} \bar{f}(r, r') dr = \sigma$$

The first term corresponds to knockout nucleons and evaporation particles so that $\alpha r' \gg 1$. The second term corresponds to the quasielastic scattered primary such that $\gamma r' \ll 1$. Typically, $\alpha \simeq 1 \rightarrow 10$ cm^2/g and $\gamma \simeq 10^{-3} \rightarrow 10^{-2}$ cm^2/g. Equation (11) will be used later when considering the simplification of the numerical procedure.

Error propagation. In considering how errors are propagated in the use of equation (10), the error is introduced locally by calculating $\psi(x, r+h)$ over the range (energy) grid. Limiting our current analysis to the first term of equation (10), at each range grid r_i it is defined that

$$\psi(x+h, r_i) = e^{-\sigma h}\ \psi(x, r_i+h) \tag{12}$$

We denote the truncation error ϵ_i introduced in the interpolation procedure to the interpolated value ψ_{int} as

$$\psi(x, r_i+h) = \psi_{\text{int}}(x, r_i+h) + \epsilon_i(h) \tag{13}$$

After the kth step from the boundary, the numerical solution is

$$\psi(kh, r_i) = e^{-\sigma h}\ \psi_{\text{int}}\left[(k-1)h, r_i+h\right] + \sum_{\ell=0}^{k-1} e^{-\sigma(k-\ell)h} \epsilon_\ell(h) \tag{14}$$

Suppose that $0 \leq \epsilon_\ell(h) \leq \epsilon(h)$ for all indexes ℓ; then the propagated (prp) error is bound by

$$\epsilon_{\text{prp}}(k) = \sum_{\ell=0}^{k-1} e^{-\sigma(k-\ell)h}\ \epsilon_\ell(h) \leq \epsilon(h) \sum_{\ell=0}^{k-1} e^{-\sigma(k-\ell)h} \tag{15}$$

We note that

$$\sum_{\ell=0}^{k-1} e^{-\sigma k h}\ e^{\sigma h \ell} \approx \frac{1}{h\sigma}\left(1 - e^{-\sigma k h}\right) \tag{16}$$

since $h\sigma \ll 1$. Clearly the propagated error on the kth step is bound by

$$\epsilon_{\text{prp}}(h) < \frac{\epsilon(h)}{h\sigma}\left(1 - e^{-\sigma k h}\right) \tag{17}$$

where $\epsilon(h)$ is the maximum error per step. With increasing values of k, the propagated error grows each step to a maximum value of $\epsilon(h)/h\sigma$. For a typical situation, if we take $h\sigma = 0.01$ and the step size $h = 1$ g/cm^2, the propagated error increased by extending the transport calculation from 30 to 150 g/cm^2 is three times as large (i.e., $\epsilon_{\text{prp}} \leq 78\ \epsilon(h)$ instead of $\epsilon_{\text{prp}} \leq 26\ \epsilon(h)$). Evidently, we need to control the truncation error at each step.

Numerical procedure. We now consider numerical methods for the integral portion of equation (8). We will make use of the form of the interaction given by equation (11) for which an analytic solution can be easily obtained. As shown in connection with equation (10), equation (8) may be rewritten as

$$\psi(x+h,r) = e^{-\sigma h}\ \psi(x,r+h) + e^{-\sigma h}\int_0^h dz \int_r^\infty dt\ ae^{-\alpha(r+z)}\ \psi(x,t+h)$$

$$+ e^{-\sigma h}\int_0^h dz \int_r^\infty dt\ ce^{\gamma(r-t-Q)}\ \psi(x,t+h) + O(h^2) \tag{18}$$

where Q represents the average energy shift of the projectile producing the secondary particles across the interval x to $x+h$ and t is a dummy variable. In principle, a, α, c, and γ are dependent on projectile energy as well and would be evaluated using the same Q value (ref. 1). With the analytic forms in equation (18) we may perform the integrals as

$$\psi(x+h,r) = e^{-\sigma h}\ \psi(x,r+h) + e^{-\sigma h}\int_r^\infty dt\ \frac{a}{\alpha}\left[e^{-\alpha r} - e^{-\alpha(r+h)}\right]\psi(x,t+h)$$

$$+ e^{-\sigma h}\int_r^\infty dt\ hce^{\gamma(r-t)}\ \psi(x,t+h) + O(h^2) \tag{19}$$

The integral terms of equation (19) can be written in terms of the cumulative secondary spectra denoted as

$$F_a(r,t) = \int_0^r ae^{-\alpha z}\ dz \tag{20}$$

and

$$F_c(r,t) = \int_0^r ce^{\gamma(z-t)}\ dz \tag{21}$$

In particular,

$$\frac{a}{\alpha}\left[e^{-\alpha r} - e^{-\alpha(r+h)}\right] = F_a(r+h,t+Q) - F_a(r,t+Q) \tag{22}$$

$$che^{\gamma(r-t-Q)} = \left[F_c(r+h,t+Q) - F_c(r,t+Q)\right]\left[1 - \frac{1}{2}\gamma(h-2Q) + O(h^2)\right] \tag{23}$$

which may now be substituted into equation (19) to obtain

$$\psi(x+h,r) = e^{-\sigma h}\ \psi(x,r+h) + e^{-\sigma h}\int_r^\infty dt\,[F_a(r+h,t+Q) - F_a(r,t+Q)]\ \psi(x,t+h)$$

$$+ e^{-\sigma h}\int_r^\infty dt\,[F_c(r+h,t+Q) - F_c(r,t+Q)]\ \psi(x,t+h) + O(h-2Q) + O(h^2) \tag{24}$$

The second-order accuracy is maintained only if Q is chosen at the midpoint of the interval (i.e., $Q = h/2$). Additional details of this analysis can be found in reference 1. The propagation equation is implemented as

$$\psi(x+h,r) = e^{-\sigma h}\ \psi(x,r+h) + \int_r^\infty dt\ \bar{F}\left(h,r,t+\frac{h}{2}\right)\ \psi(x,t+h) \tag{25}$$

where

$$\bar{F}(h,r,t) = \int_0^h \bar{f}(r+z,t)\ dz$$

$$\equiv F(r+h,t) - F(r,t) \tag{26}$$

and is related to the cumulative energy spectrum by

$$F(r,t) = \int_0^{\epsilon(r)} f(E,E')\ dE \tag{27}$$

where $\epsilon(r)$ is the energy associated with the residual range r and $E' = \epsilon(t)$.

Coupled Baryon Transport

The coupled baryon transport equations are of the form

$$\left[\frac{\partial}{\partial x} - \nu_j \frac{\partial}{\partial E} S(E) + \sigma_j(E)\right]\ \phi_j(x,E) = \sum_k \int_0^\infty f_{jk}(E,E')\ \phi_k(x,E')\ dE' \tag{28}$$

where ν_j is the range scaling parameter, $S(E)$ is the proton stopping power, $\sigma_j(E)$ is the total cross section, $\phi_j(x,E)$ is the differential flux spectrum of type j baryons, and $f_{jk}(E,E')$ is a differential energy cross section for the redistribution of particle type and energy. Utilizing the definitions

$$r = \int_0^E dE'/S(E') \tag{29}$$

$$\psi_j(x,r) = S(E)\ \phi_j(x,E) \tag{30}$$

and

$$\bar{f}_{jk}(r,r') = S(E)\ f_{jk}(E,E') \tag{31}$$

allows equation (28) to be written as

$$\left[\frac{\partial}{\partial x} - \nu_j \frac{\partial}{\partial r} + \sigma_j(r)\right] \psi_j(x,r) = \sum_k \int_r^\infty \bar{f}_{jk}(r,r')\ \psi_k(x,r')\ dr' \tag{32}$$

which may be rewritten (refs. 5 and 10) as

$$\psi_j(x,r) = e^{-\zeta_j(r,x)}\ \psi_j(0,r+\nu_j x) + \sum_k \int_0^x \int_r^\infty e^{-\zeta_j(r,z)}\ \bar{f}_{jk}(r+\nu_j z,r')\ \psi_k(x-z,r')\ dr'\ dz \tag{33}$$

where the exponential is the integrating factor with

$$\zeta_j(r,t) = \int_0^t \sigma_j(r+\nu_j t')\ dt' \tag{34}$$

In case of $j = n$ (neutron), $\zeta_j(r,t)$ reduces to $\sigma_n(r)\,t$ since $\nu_n = 0$.

Rather simple numerical procedures follow from equation (33). Noting that the first-order nature of equation (28) allows $\psi_j(x,r)$ to be taken as a boundary condition for propagation to larger values of x, one may approximate equation (33) as

$$\psi_j(x+h,r) = e^{-\zeta_j(r,h)}\ \psi_j(x,r+\nu_j h) + \sum_k \int_0^h \int_r^\infty e^{-\zeta_j(r,z)}\ \bar{f}_{jk}(r+\nu_j z,r')\ \psi(x+h-z,r')\ dz\ dr' \tag{35}$$

which may be used to develop a numerical stepping procedure. Equation (35) has provided the basis for a number of new transport codes for baryons of mass number greater than or equal to 1 (ref. 8). These codes are now being extended to couple with the meson fields and to the negative baryon number fields.

If h is sufficiently small that

$$\sigma_j(r')\ h \ll 1 \tag{36}$$

then, according to perturbation theory (ref. 5),

$$\psi_k(x+h-z,r') \approx e^{-\zeta_k(r,h-z)}\ \psi_k[x,r'+\nu_k(h-z)] \tag{37}$$

which may be used to approximate the aforementioned integral of equation (35).

For many cases of practical interest (e.g., accelerator studies), monoenergetic particle beams are used, and thus separation of the singular terms from the solution becomes convenient. The initial beam of type J particles of energy E_0 (where $r_0 = R(E_0)$) is taken as

$$\psi_j(0,r) = \delta_{jJ}\delta(r_0 - r) \tag{38}$$

and the solution is written as

$$\psi_j(x,r) = \psi_{j0}(x,r) + \psi_j(x,r) \tag{39}$$

The corresponding singular terms are

$$\psi_{k0}(x,r) = e^{-\zeta_k(r,x)}\delta(r_0 - r - \nu_k x)\delta_{kj} \tag{40}$$

The regular terms of equation (35) for $k = p$ may be written as

$$\psi_p(x+h,r) = e^{-\zeta_p(r,h)}\ \psi_p(x,r+h) + \int_0^h dz\ e^{-\zeta_p(r,z)} \sum_j \int_{r+z}^{\infty} \bar{f}_{pj}(r+z,r')\ [\psi_{j0}(x+h-z,r')$$

$$+ \psi_j(x+h-z,r')]\ dr' \tag{41}$$

and the regular terms for $k = n$ are

$$\psi_n(x+h,r) = e^{-\sigma_n(r)\,h}\ \psi_n(x,r) + \int_0^h dz\ e^{-\sigma_n(r)\,z} \sum_j \int_r^{\infty} \bar{f}_{nj}(r,r')\ [\psi_{j0}(x+h-z,r')$$

$$+ \psi_j(x+h-z,r')]\ dr' \tag{42}$$

The singular contribution under the integrals of equations (41) and (42) can be evaluated with equation (40), and the approximations in equations (36) and (37) can be applied to find

$$\psi_p(x+h,r) = \exp[-\sigma_p(r)\,h]\ \psi_p(x,r+h) + \exp\left\{-[\sigma_p(r) + \sigma_p(r'_0)]\frac{h}{2}\right\}\ \bar{F}_{pp}(h,r,r'_0)\ \delta_{pj}\ \exp[-\zeta_p(r'_0,x)]$$

$$+ \exp\left\{-[\sigma_p(r) + \sigma_n(r_0)]\frac{h}{2}\right\}\ \bar{F}_{pn}(h,r,r_0)\ \delta_{nj}\ \exp[-\sigma_n(r_0)x]$$

$$+ \int_r^{\infty} \exp\left\{-\left[\sigma_p(r) + \sigma_p\left(r' + \frac{h}{2}\right)\right]\frac{h}{2}\right\} \bar{F}_{pp}\left(h,r,r'+\frac{h}{2}\right) \psi_p(x,r'+h)\ dr'$$

$$+ \int_r^{\infty} \exp\left\{-\left[\sigma_p(r) + \sigma_n\left(r' + \frac{h}{2}\right)\right]\frac{h}{2}\right\} \bar{F}_{pn}\left(h,r,r'+\frac{h}{2}\right) \psi_n\left(x,r'+\frac{h}{2}\right) dr' \tag{43}$$

and

$$\psi_n(x+h,r) = \exp[-\sigma_n(r)\,h]\;\psi_n(x,r) + h\;\bar{f}_{np}(r,r'_0)\;\exp\left\{-[\sigma_n(r)+\sigma_p(r'_0)]\frac{h}{2}\right\}\delta_{pj}\;\exp[-\zeta_p(r'_0,x)]$$

$$+ h\;\bar{f}_{nn}(r,r'_0)\;\exp\left\{-[\sigma_n(r)+\sigma_n(r_0)]\frac{h}{2}\right\}\delta_{nj}\;\exp[-\sigma_n(r_0)\;x]$$

$$+ h\int_r^\infty \exp\left\{-[\sigma_n(r)+\sigma_p(r')]\frac{h}{2}\right\}\;\bar{f}_{np}(r,r')\;\psi_p\left(x,r'+\frac{h}{2}\right)dr'$$

$$+ h\int_r^\infty \exp\left\{-[\sigma_n(r)+\sigma_n(r')]\frac{h}{2}\right\}\;\bar{f}_{nn}(r,r')\;\psi_n(x,r')\;dr' \tag{44}$$

where $r'_0 = r_0 - x - \frac{h}{2}$ and $\bar{F}$ is related to the cumulative spectrum F as given by

$$\bar{F}_{ij}(h,r,r') = \int_0^h \bar{f}_{ij}(r+z,r')\;dz$$

$$\equiv F_{ij}(r+h,r') - F_{ij}(r,r') \tag{45}$$

with

$$F_{ij}(r,r') = \int_0^{\epsilon(r)} f_{ij}(E,E')\;dE \tag{46}$$

where $\epsilon(r)$ is the energy associated with residual range r and $E' = \epsilon(r')$. Equations (43) and (44) are evaluated by establishing an x-grid at which $\psi_j(x_m,r)$ is evaluated where h is the distance between each successive evaluation. The integral over r' is accomplished by establishing an r-grid (and the corresponding E-grid) and using

$$\int_{r_n}^\infty g(r_n,r')\;\psi_j(x_m,r')\;dr' \approx \sum_{\ell=n}^\infty g_n(r_n,\bar{r}_\ell)\;\int_{r_\ell}^{r_{\ell+1}} \psi_j(x_m,r)\;dr' \tag{47}$$

where $\bar{r}_\ell = (r_\ell + r_{\ell+1})/2$, and the series terminates at the highest ℓ value in the r-grid which is related to the maximum range (energy) cutoff $r_{\max}$.

Numerical Algorithms

The error analysis shown earlier has demonstrated the need for controlling the local truncation errors so that the application of BRYNTRN can be extended to a very thick shield. Although the analysis was limited to the attenuation of the primary particles (the first term of eq. (10)), the contribution of error from evaluating the generation of secondaries is also significant. Restricting our scope presently to the space application, we focus only on the numerical algorithms in treating the first, fourth, and fifth terms of equations (43) and (44). The first term requires interpolation of ψ, the rest involve both interpolation and numerical integration. Furthermore, since the number of range (energy) grids is limited by the computational efficiency, the distribution of grids should be optimized.

The existing interpolation algorithms in the code consist of either the second-order Lagrange methods or a scheme assuming a solar-proton-fluence spectrumlike function for ψ with two parameters determined by the two neighboring points. These algorithms were adequate for a propagating distance of approximately 30 g/cm^2 (ref. 4). To improve further, a choice is made from a host of interpolation methods existing in the literature (refs. 11–13). Among them, a good candidate is the third-order Lagrange method with the four neighboring grid points placed evenly on both sides of the specified (interpolated) point. If the distribution of grids is rather uniform (on a logarithm scale that is suitable for the space radiation spectrum), the error will tend to be the smallest in the middle interval of all the data points (ref. 11). The choice of a much higher order Lagrange method will substantially decrease the efficiency of the code

since there are more than 10 interpolation calls for each single-energy point at every step. Other interpolation methods such as the cubic spline were considered but discarded. The splines are, in general, more accurate. However, their characteristic large excursions (oscillations) can result in unpredictable erroneous solutions.

The numerical integration procedures are used not only for evaluating the secondaries-generation terms but also for calculating the dose and dose equivalent. The existing procedure is based on the compound quadrature formula summing over all the subintervals between the midpoints of the grids. The same proton-fluence spectrumlike function as that described earlier for an existing interpolation procedure was assumed for each interval. Clearly, this assumption has the advantage of providing an analytic expression for the integration over the subintervals, but it has less-accurate interpolated values. The new integration procedure proposed will retain the nature of compound quadrature formulation and make use of the improved interpolation procedures mentioned earlier. To replace the analytical integration for the subintervals, a simple numerical method such as Simpson's rule is suggested.

In the existing code, the generation of range grids is based on the uniform logarithm energy spacings. This choice was motivated by the fact that the solar proton fluences are usually several orders of magnitude larger at the low-energy end of the spectrum. Also, the main contribution of the doses usually comes from the large stopping power at the low-energy region where the protons are near the end of their tracks; therefore more numerical precision is needed for the low-energy region. With the interpolation procedure replaced by the third-order Lagrange method, changes must be made to ensure that the logarithm grids will be uniform in range rather than in energy. Further modification can be made to minimize the number of grid points so that the efficiency of the code can be improved.

Note that the information propagating through the steps is carried from the interpolated r_i+h points to the r_i-grids of the next step. Since h is usually taken to be about 1 g/cm^2 and the range grids cover the scale roughly from 10^{-4} to 10^3 g/cm^2, the fraction of grid points below $r_{\min}+h$ that are not used as data points in interpolation and that, consequently, are not carrying information downstream can be substantial. Hence, the modification can be made to distribute fewer points below 1 g/cm^2. Note that all the grid-generation options mentioned here have several closely spaced points concentrated at the very high energy end of the logarithm scale.

Results and Discussion

The existing and new algorithms for interpolation and integration, plus various grid-distribution options, are tested and compared for several solar-flare proton spectra. These spectra are presented as follows (refs. 14–18):

1. The February 1956 solar particle event (SPE):

$$\phi_P(>E) = 1.5 \times 10^9 \exp\left(-\frac{E-10}{25}\right) + 3 \times 10^8 \exp\left(-\frac{E-100}{320}\right)$$

2. The November 1960 SPE:

$$\phi_P(>E) = 7.6 \times 10^9 \exp\left(-\frac{E-10}{12}\right) + 3.9 \times 10^8 \exp\left(-\frac{E-100}{80}\right)$$

3. The August 1972 SPE:

$$\phi_P(>E) = 6.6 \times 10^8 \exp\left(-\frac{E-100}{30}\right)$$

4. The August 1972 SPE (King spectrum):

$$\phi_P(>E) = 7.9 \times 10^9 \exp\left(-\frac{E-30}{26.5}\right)$$

5. A Webber spectrum with 100 MV rigidity:

$$\phi_P(>E) = 1.0 \times 10^9 \exp\left[\frac{239.1-P(E)}{100}\right]$$

6. The August 1989 SPE:

$$\phi_P(>E) = 8.65 \times 10^{10} \exp\left[-\frac{P(E)}{59.261}\right]$$

where E is the energy (in units of MeV), $P(E) = \sqrt{E(E+1876)}$, and $\phi_P(>E)$ is the proton integral fluence (in units of protons/cm^2).

Since the Lagrange methods are sensitive to the grid distribution, the truncation errors introduced by interpolating the spectrum are compared for various combinations of interpolation procedures and grid-distribution options. Figures 1–5 show the fractional error of interpolated function $\psi(0, r_i + h)$ at each r_i-grid for the above-listed spectra 1–5, respectively. The interpolating distance h is either 0.5 (figs. 1(a)–5(a)) or 1 g/cm^2 (figs. 1(b)–5(b)). It is seen that for all the spectra and h values tested, the combination of existing (uniform logarithm E) grid and the second-order Lagrange method results in the largest error. (Note that although it is not shown here, the interpolation error for the other existing algorithm assuming a solar-proton-fluence spectrum-like function was found to be even larger.) Progressively improved accuracy is seen when the second-order Lagrange method is replaced by the third-order method and the uniform logarithm E-grid is replaced by the uniform logarithm r-grid, and subsequently by the modified logarithm r-grid. As mentioned earlier, the modified grid distribution has fewer grid points below 1 g/cm^2 in range. Consequently, it gives less spacing between the data points that are used for interpolation, thus resulting in better accuracy. Table 1 lists the maximum percentage error of interpolation for the existing (old) and new methods (modified uniform r-grid and third-order Lagrange, respectively). The overall improvement is at least a factor of 10 to 20 with all the spectra tested.

A comparison is also made of the new and existing (old) integration procedures. Fractional differences in the results between analytical and numerical integration of ψ from r_i to $r_{\max}$ are shown in figure 6 for the February 1956 SPE spectrum. Drastic improvement is seen for the new algorithm with an accuracy of ± 0.05 percent or less. This is probably attributed to the improved interpolation method used in the new integration procedure. The fairly "simple-minded" numerical integration, such as Simpson's rule used for the subintervals, is obviously not a concern here.

To test the numerical convergence in solutions obtained by using the new algorithms for interpolation, integration, and grid generation, sample dose calculations are made through a very thick shield. Figure 7(a) shows various components of free-space absorbed dose as a function of aluminum thickness up to 150 g/cm^2 for the August 1989 SPE spectrum. These results are obtained by using the number of r-grid points $N = 30$. Similar results obtained with $N = 60$ and $N = 90$ (figs. 7(b) and 7(c), respectively) show practically no difference from those with $N = 30$, and therefore convergence is quite evident. To examine in further detail, the $N = 30$ and $N = 60$ results relative to the $N = 90$ results are compared for each individual dose component. (See fig. 8.) In general, it appears that the relative errors increase as the number of propagating steps increases, as expected. The maximum relative error for the $N = 60$ results is approximately 1.5 percent excluding the secondary-neutron high-energy heavy ion (HZE) recoil dose where there is an oscillatory behavior in the converging solution as the number of grids increases. The relative error for $N = 30$ is approximately 3.5 percent except for the secondary-proton ionization dose where the ramping error against the increasing shield thickness is large and reaches about 10 percent. To reduce such ramping, the number of grid points below 1 g/cm^2 was further reduced for $N = 30$ by either changing the grid-generation formula or merely increasing the maximum energy cutoff from 1000 to 4000 MeV. In both cases, the results show a considerable reduction in maximum error to less than 5 percent.

The oscillatory behavior in the converging solutions for the secondary-neutron HZE recoil dose probably came from the rapidly varying cross-section data (ref. 1) for neutrons at the low energy. This is also indicated in the less-smooth distribution curve of ψ for the secondary neutrons at distances farther from the boundary. (See fig. 9.)

Other results obtained that also show the accuracy of the new algorithms are given in tables 2 and 3. The calculations were intended for predicting the skin dose received by the aircraft passengers at various altitudes. For economical reasons, the results with $N = 60$ are available only to a thickness of air of 150 g/cm^2. The difference between the $N = 30$ and $N = 60$ results is almost negligible.

Another convergence issue that needs to be addressed is the perturbation series for the nucleon transport method used here. The perturbation theory requires that $\sigma h \ll 1$. Since $\sigma = 0.01$ cm^2/g, we usually take $h = 1$ g/cm^2. Although the numerical error has been reduced considerably to about 5 percent for the large shield thickness, the error from the perturbation series should also be brought in line. By varying the value of h down to 0.1 g/cm^2, it is demonstrated that the solution converges rather quickly as shown in figure 10. Without sacrificing much computing time, a step size of 0.5 g/cm^2 appears to be a reasonable choice for an error of approximately 10 percent for the secondaries. The overall computing time is found to be about the same as it was when using the old algorithms for the same number of grid points. Note that the test for convergence (conducted by the third author) using the old

algorithm indicates (see fig. 11) an order-of-magnitude difference in the secondary-neutron results for large shield thickness for the same case as that computed for figure 7. As mentioned earlier, the old algorithms were adequate for a thickness up to about 30 g/cm^2 as shown in figure 11, but they should be replaced with the new algorithms described herein.

Concluding Remarks

The use of the baryon transport computer code (BRYNTRN) in space radiation dose analyses for very large shield thicknesses is improved by modifying the numerical algorithms. These include interpolation, numerical integration, and grid-generation procedures. An accuracy of approximately 5 percent for a shield thickness of 150 g/cm^2 was found when a minimal 30-point energy grid was used. Future efforts should be placed on improving the nuclear data base and adding meson contributions.

NASA Langley Research Center
Hampton, VA 23665-5225
March 20, 1991

References

1. Wilson, John W.; Townsend, Lawrence W.; Nealy, John E.; Chun, Sang Y.; Hong, B. S.; Buck, Warren W.; Lamkin, S. L.; Ganapol, Barry D.; Khan, Ferdous; and Cucinotta, Francis A.: *BRYNTRN: A Baryon Transport Model.* NASA TP-2887, 1989.

2. Townsend, Lawrence W.; Nealy, John E.; Wilson, John W.; and Atwell, William: Large Solar Flare Radiation Shielding Requirements for Manned Interplanetary Mission. *J. Spacecr. & Rockets*, vol. 26, no. 2, Mar./Apr. 1989, pp. 126–128.

3. Nealy, John E.; Wilson, John W.; and Townsend, Lawrence W.: *Preliminary Analyses of Space Radiation Protection for Lunar Base Surface Systems.* SAE Tech. Paper Ser. 891487, July 1989.

4. Shinn, Judy L.; Wilson, John W.; Nealy, John E.; and Cucinotta, Francis A.: *Comparison of Dose Estimates Using the Buildup-Factor Method and a Baryon Transport Code (BRYNTRN) With Monte Carlo Results.* NASA TP-3021, 1990.

5. Wilson, John W.; and Lamkin, Stanley L.: Perturbation Theory for Charged-Particle Transport in One Dimension. *Nucl. Sci. & Eng.*, vol. 57, no. 4, Aug. 1975, pp. 292–299.

6. Wilson, John W.; and Townsend, Lawerence W.: Radiation Safety in Commercial Air Traffic: A Need for Further Study. *Health Phys.*, vol. 55, no. 6, Dec. 1988, pp. 1001–1003.

7. Foelsche, Trutz; Mendell, Rosalind B.; Wilson, John W.; and Adams, Richard R.: *Measured and Calculated Neutron Spectra and Dose Equivalent Rates at High Altitudes; Relevance to SST Operations and Space Research.* NASA TN D-7715, 1974.

8. Wilson, John W.; Townsend, Lawrence W.; Ganapol, Barry; Chun, Sang Y.; and Buck, Warren W.: Charged-Particle Transport in One Dimension. *Nucl. Sci. & Eng.*, vol. 99, no. 3, July 1988, pp. 285–287.

9. Wilson, John W.; Townsend, Lawrence W.; Chun, Sang Y.; Buck, Warren W.; Khan, Ferdous; and Cucinotta, Frank: *BRYNTRN: A Baryon Transport Computer Code—Computation Procedures and Data Base.* NASA TM-4037, 1988.

10. Wilson, John W.; and Badavi, F. F.: Methods of Galactic Heavy Ion Transport. *Radiat. Res.*, vol. 108, 1986, pp. 231–237.

11. Yakowitz, Sidney; and Szidarovszky, Ferenc: *An Introduction to Numerical Computations, Second ed.* Macmillan Publ. Co., c.1989.

12. Johnson, Lee W.; and Riess, R. Dean: *Numerical Analysis.* Addison-Wesley Publ. Co., Inc., 1977.

13. Rice, John R.: *Numerical Methods, Software, and Analysis.* McGraw-Hill, Inc., c.1983.

14. Wilson, John W.: Environmental Geophysics and SPS Shielding. *Workshop on the Radiation Environment of the Satellite Power System,* Walter Schimmerling and Stanley B. Curtis, eds., LBL-8581, UC-41 (Contract W-7405-ENG-48), Univ. of California, Sept. 15, 1978, pp. 33–116.

15. King, Joseph H.: Solar Proton Fluences for 1977-1983 Space Missions. *J. Spacecr. & Rockets*, vol. 11, no. 6, June 1974, pp. 401–408.

16. Scott, W. Wayne; and Alsmiller, R. G., Jr.: *Comparisons of Results Obtained With Several Proton Penetration Codes—Part II.* ONRL-RSIC-22, U.S. At. Energy Commission, June 1968.

17. Scott, W. Wayne; and Alsmiller, R. G., Jr.: *Comparisons of Results Obtained With Several Proton Penetration Codes.* ORNL-RSIC-17, U.S. At. Energy Commission, July 1967.

18. Nealy, John E.; Simonsen, Lisa C.; Sauer, Herbert H.; Wilson, John W.; and Townsend, Lawrence W.: *Space Radiation Dose Analysis for Solar Flare of August 1989.* NASA TM-4229, 1990.

Table 1. Maximum Error of Interpolation for Existing and New Methods

Spectrum	Maximum error of interpolation, percent, for—			
	Step size = 0.5 g/cm^2		Step size = 1 g/cm^2	
	Old algorithms	New algorithms	Old algorithms	New algorithms
1	−2.09	0.08	−3.39	0.14
2	−3.90	.19	4.05	.32
3	1.16	.05	1.90	.08
4	1.32	.06	2.16	.09
5	.40	.04	.66	.06

Table 2. Dose in Skin Tissue Behind Various Thicknesses of Air for the February 1956 SPE Spectrum

[N denotes the number of grid points used in calculation; HZE denotes high-energy heavy ion]

Thickness, g/cm^2	Dose with $N = 30$, Gy	Dose with $N = 60$, Gy	Difference, percent
Primary-proton ionization			
2	2.981	2.975	0.19
20	1.220×10^{-1}	1.219×10^{-1}	.11
50	5.767×10^{-2}	5.763×10^{-2}	.07
100	3.017×10^{-2}	3.014×10^{-2}	.10
150	1.731×10^{-2}	1.727×10^{-2}	.23
Secondary-proton ionization			
2	3.707×10^{-2}	3.694×10^{-2}	0.35
20	2.011×10^{-2}	1.994×10^{-2}	.82
50	2.345×10^{-2}	2.325×10^{-2}	.84
100	2.144×10^{-2}	2.119×10^{-2}	1.17
150	1.717×10^{-2}	1.692×10^{-2}	1.48
Secondary-neutron HZE recoil			
2	8.766×10^{-5}	8.762×10^{-5}	0.05
20	1.839×10^{-4}	1.848×10^{-4}	.46
50	2.805×10^{-4}	2.843×10^{-4}	1.35
100	3.137×10^{-4}	3.209×10^{-4}	2.30
150	2.837×10^{-4}	2.918×10^{-4}	2.85

Table 3. Dose Equivalent in Skin Tissue Behind Various Thicknesses of Air for the February 1956 SPE Spectrum

[N denotes the number of grid points used in calculation; HZE denotes high-energy heavy ion]

Thickness, g/cm^2	Dose equivalent with $N = 30$, Sv	Dose equivalent with $N = 60$, Sv	Difference, percent
Primary-proton ionization			
2	4.925	4.927	0.05
20	1.418×10^{-1}	1.418×10^{-1}	.04
50	6.205×10^{-2}	6.201×10^{-2}	.06
100	3.199×10^{-2}	3.196×10^{-2}	.10
150	1.826×10^{-2}	1.823×10^{-2}	.16
Secondary-proton ionization			
2	9.118×10^{-2}	9.110×10^{-2}	0.09
20	2.917×10^{-2}	2.895×10^{-2}	.75
50	3.105×10^{-2}	3.080×10^{-2}	.80
100	2.726×10^{-2}	2.696×10^{-2}	1.11
150	2.146×10^{-2}	2.116×10^{-2}	1.14
Secondary-neutron HZE recoil			
2	1.753×10^{-3}	1.752×10^{-3}	0.04
20	3.678×10^{-3}	3.696×10^{-3}	.47
50	5.610×10^{-3}	5.686×10^{-3}	1.33
100	6.275×10^{-3}	6.419×10^{-3}	2.25
150	5.675×10^{-3}	5.836×10^{-3}	2.77

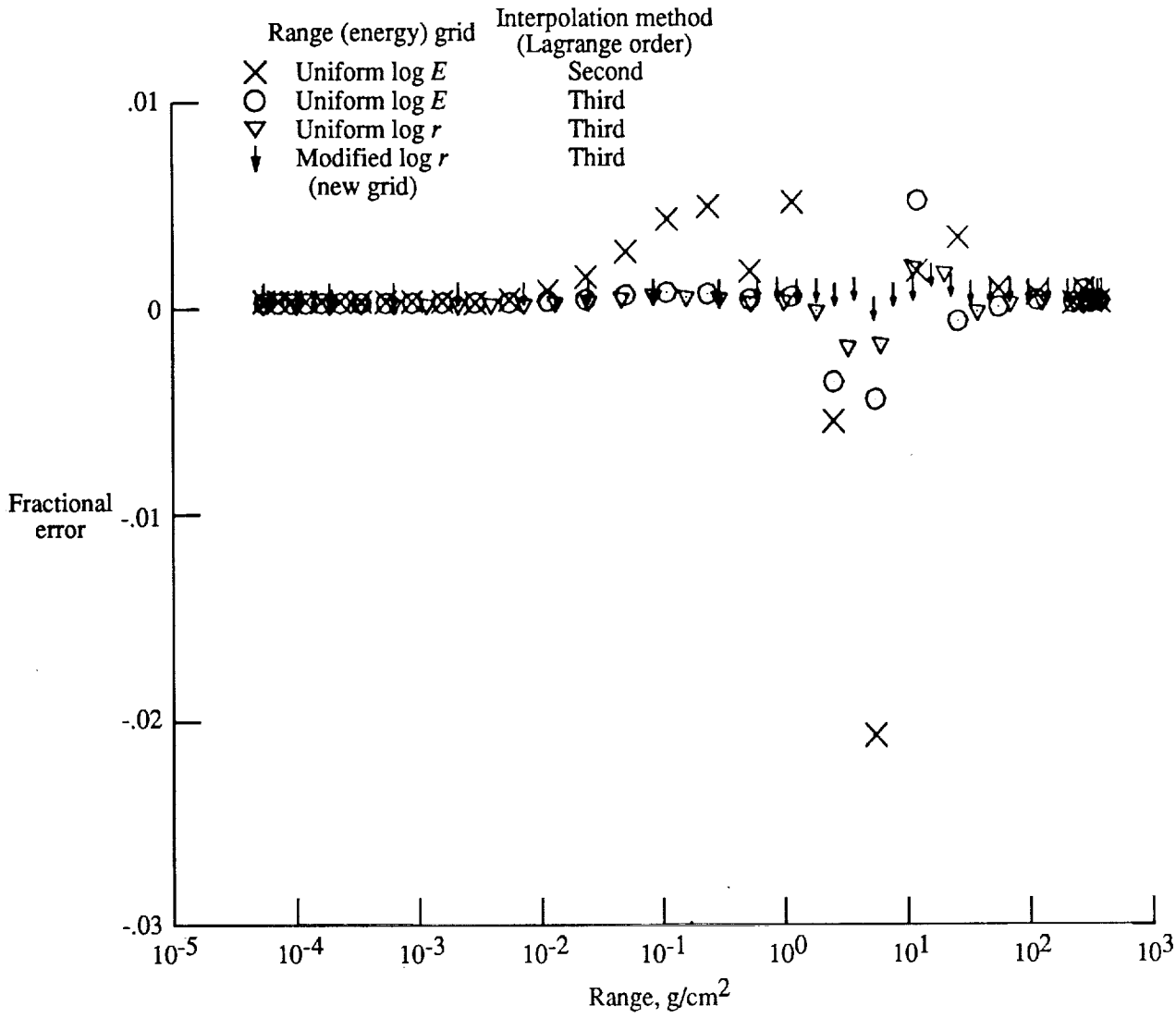

(a) $h = 0.5$ g/cm^2.

Figure 1. Fractional error of interpolating the February 1956 SPE spectrum for various grid distributions and interpolation methods.

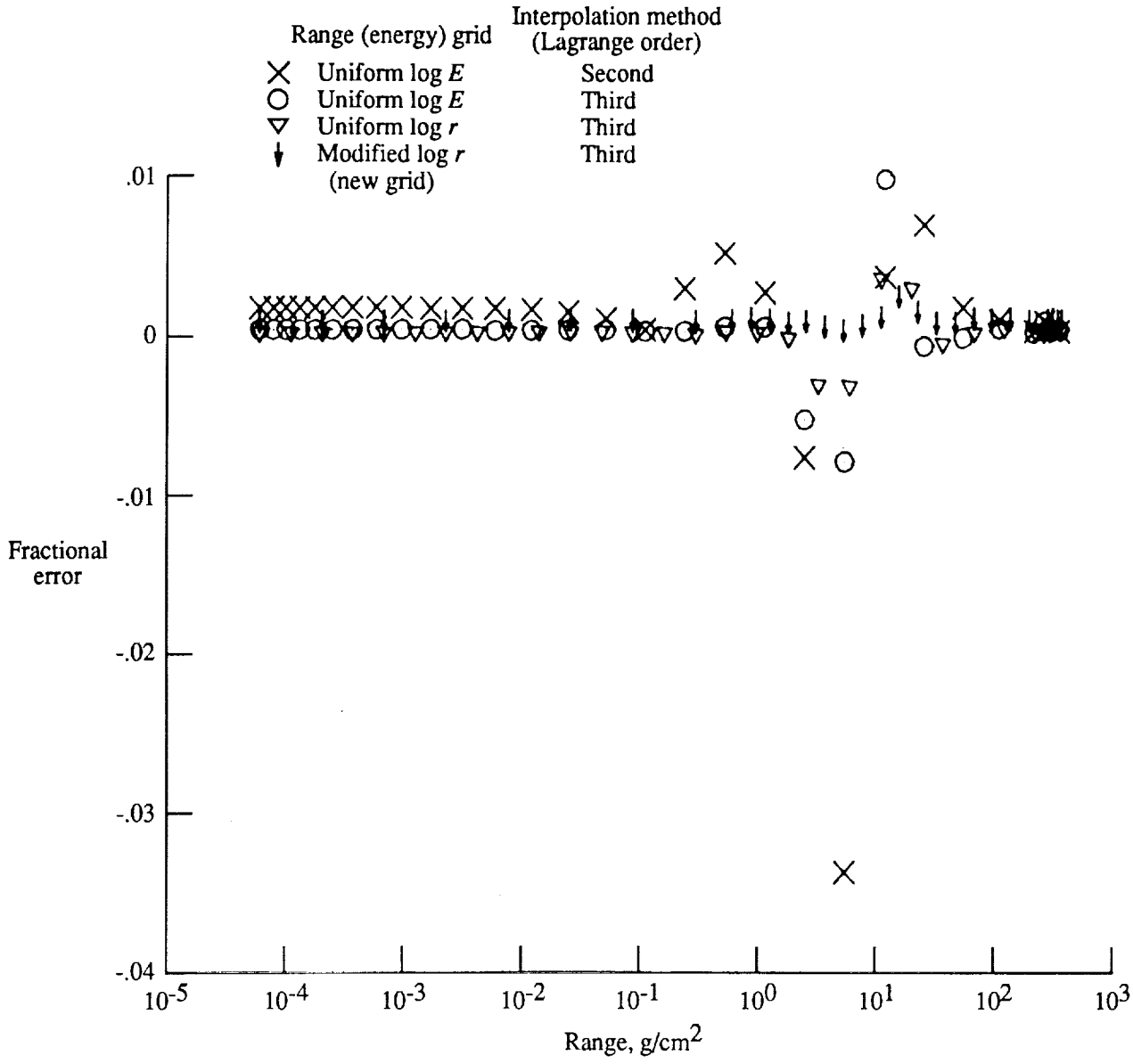

(b) $h = 1$ g/cm^2.

Figure 1. Concluded.

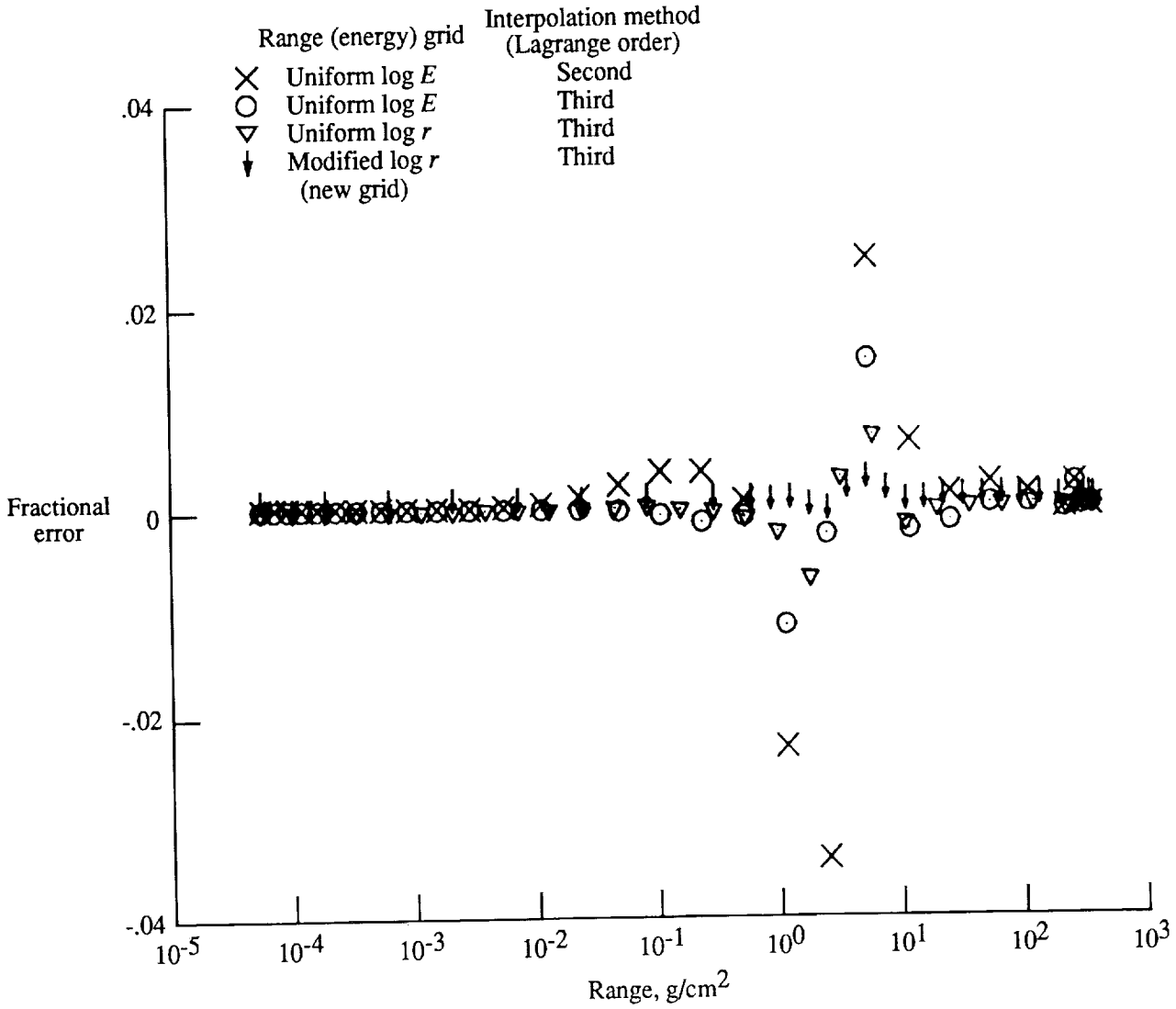

(a) $h = 0.5$ g/cm^2.

Figure 2. Fractional error of interpolating the November 1960 SPE spectrum for various grid distributions and interpolation methods.

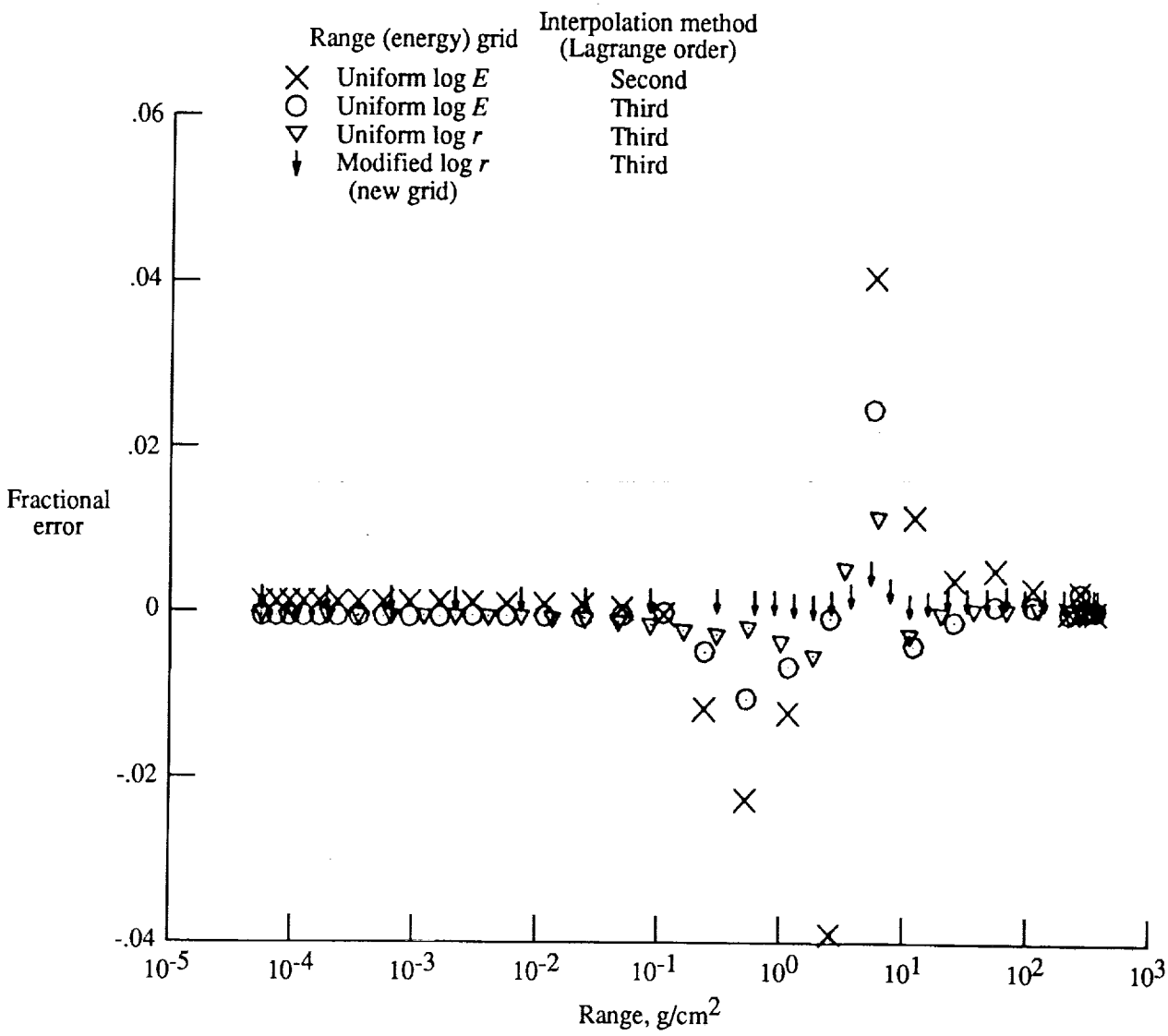

(b) $h = 1$ g/cm^2.

Figure 2. Concluded.

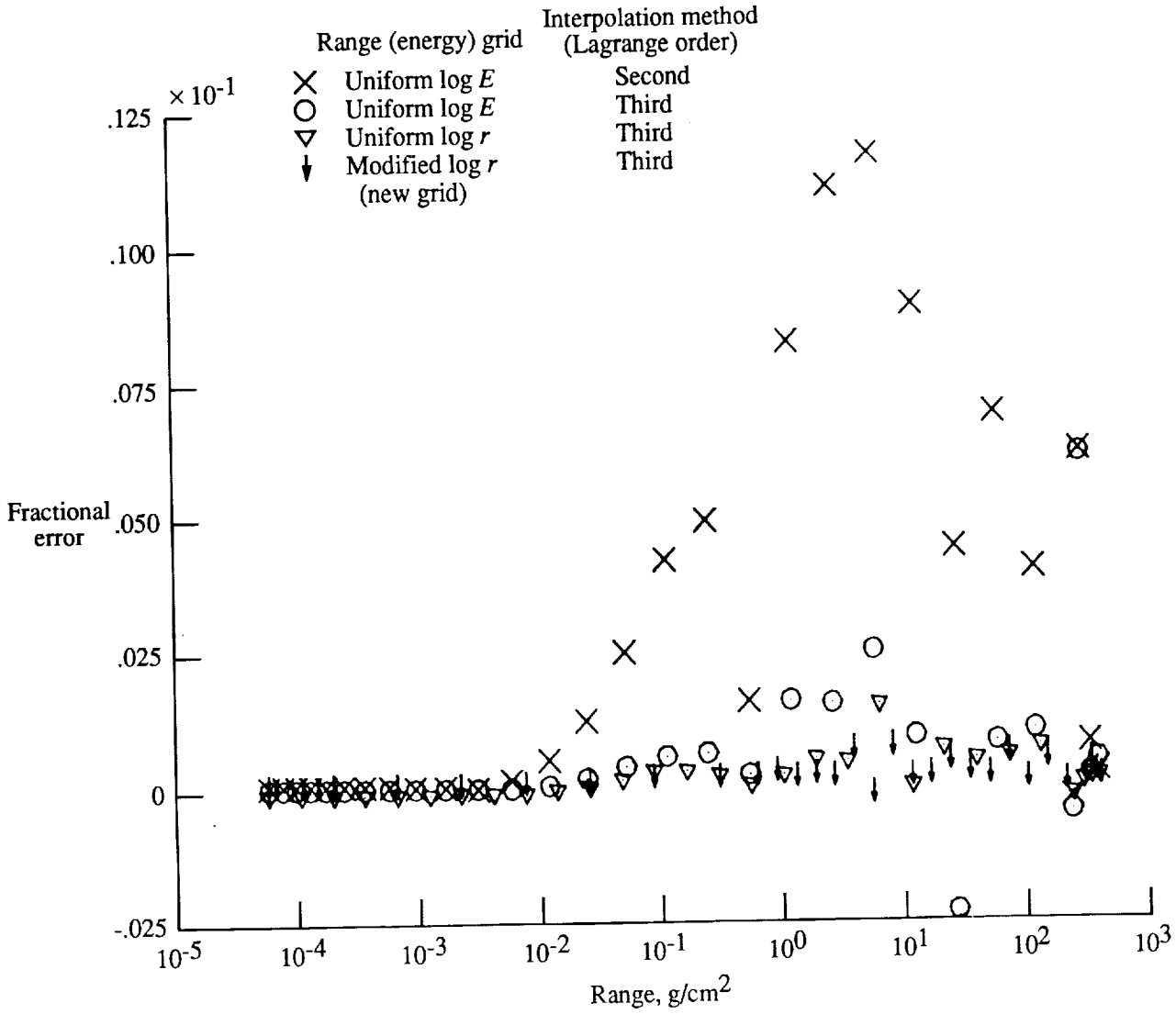

(a) $h = 0.5$ g/cm^2.

Figure 3. Fractional error of interpolating the August 1972 SPE spectrum for various grid distributions and interpolation methods.

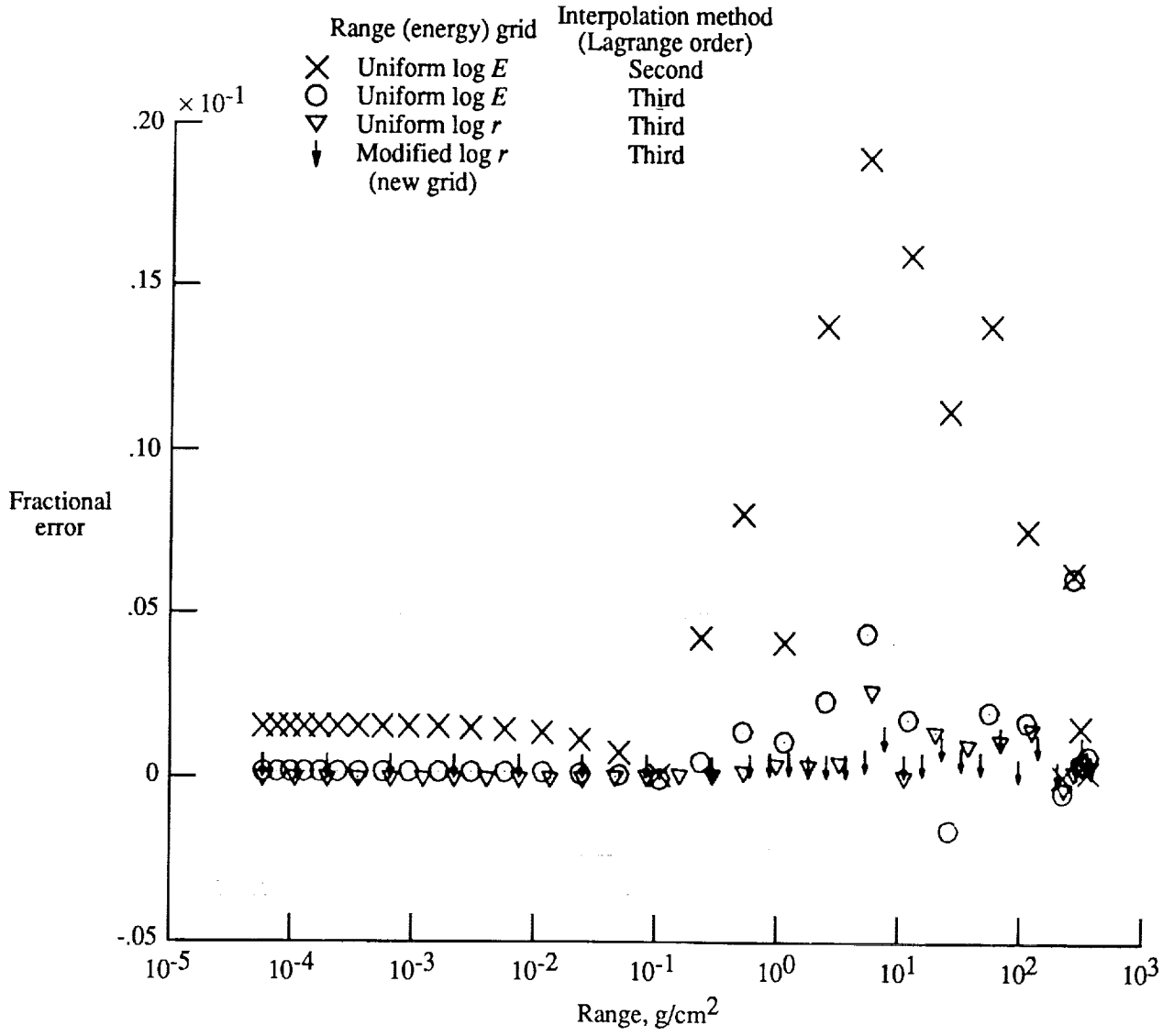

(b) $h = 1$ g/cm^2.

Figure 3. Concluded.

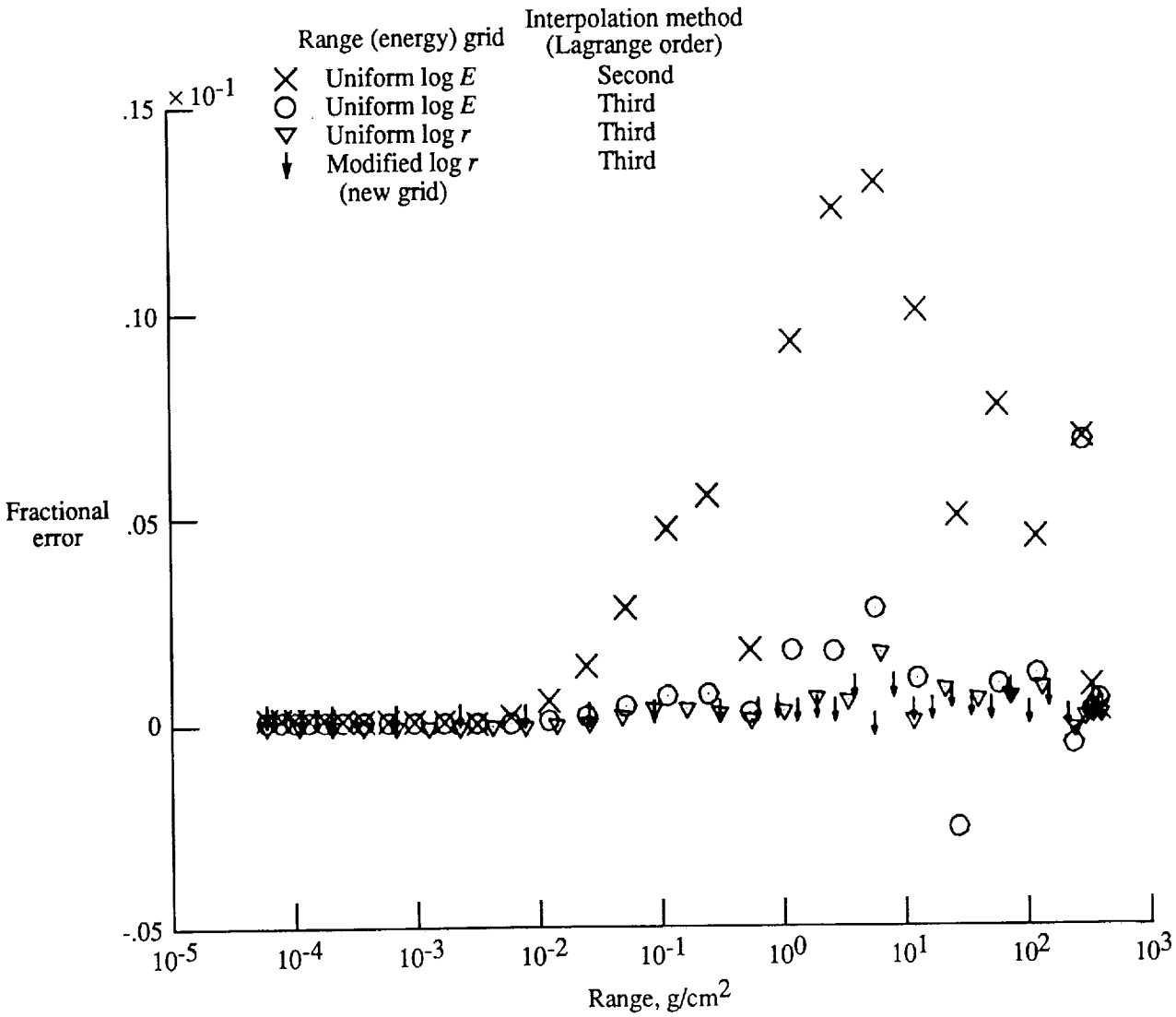

(a) $h = 0.5$ g/cm^2.

Figure 4. Fractional error of interpolating the August 1972 SPE (King) spectrum for various grid distributions and interpolation methods.

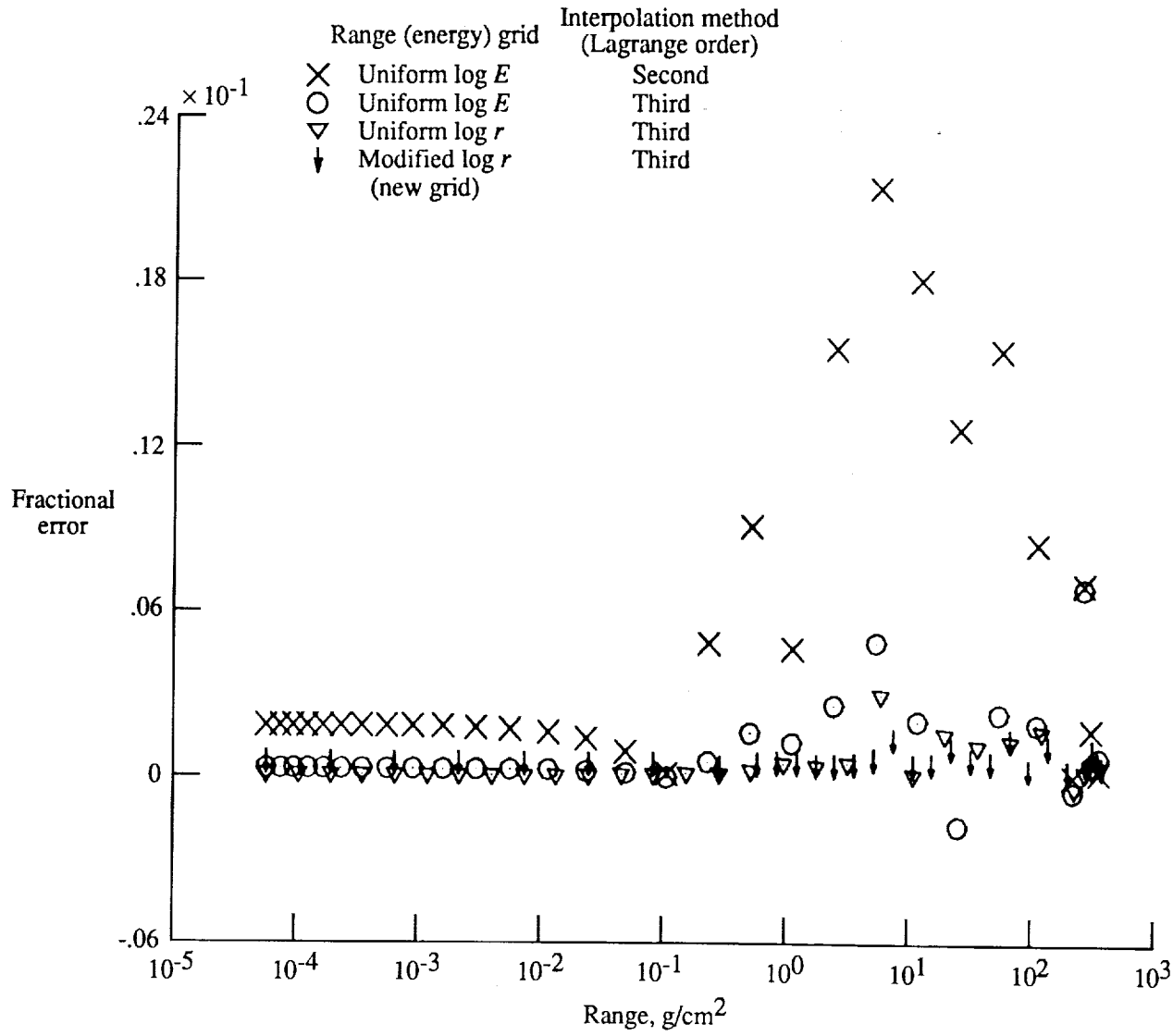

(b) $h = 1$ g/cm^2.

Figure 4. Concluded.

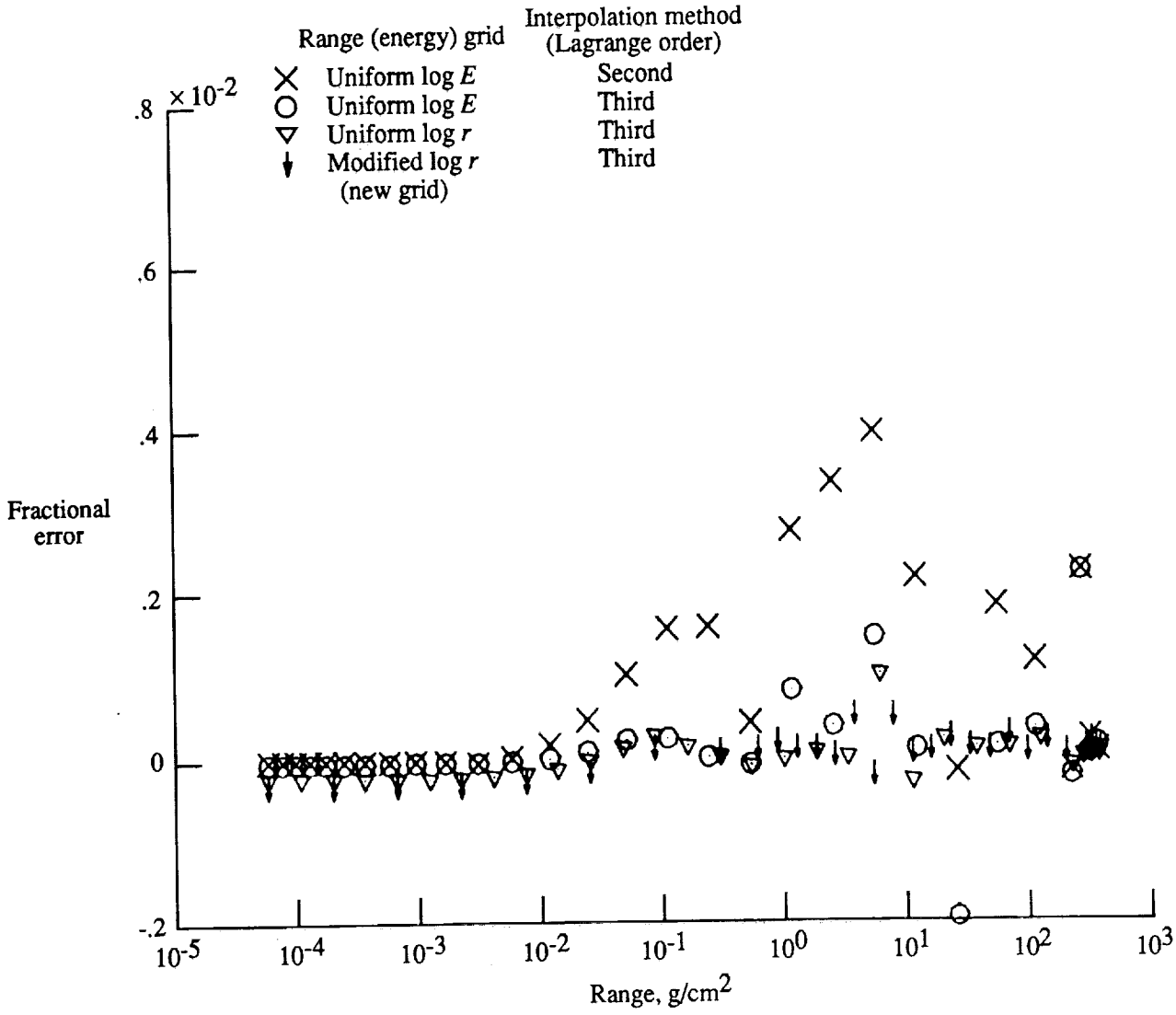

(a) $h = 0.5$ g/cm^2.

Figure 5. Fractional error of interpolating the Webber spectrum (100 MV rigidity) for various grid distributions and interpolation methods.

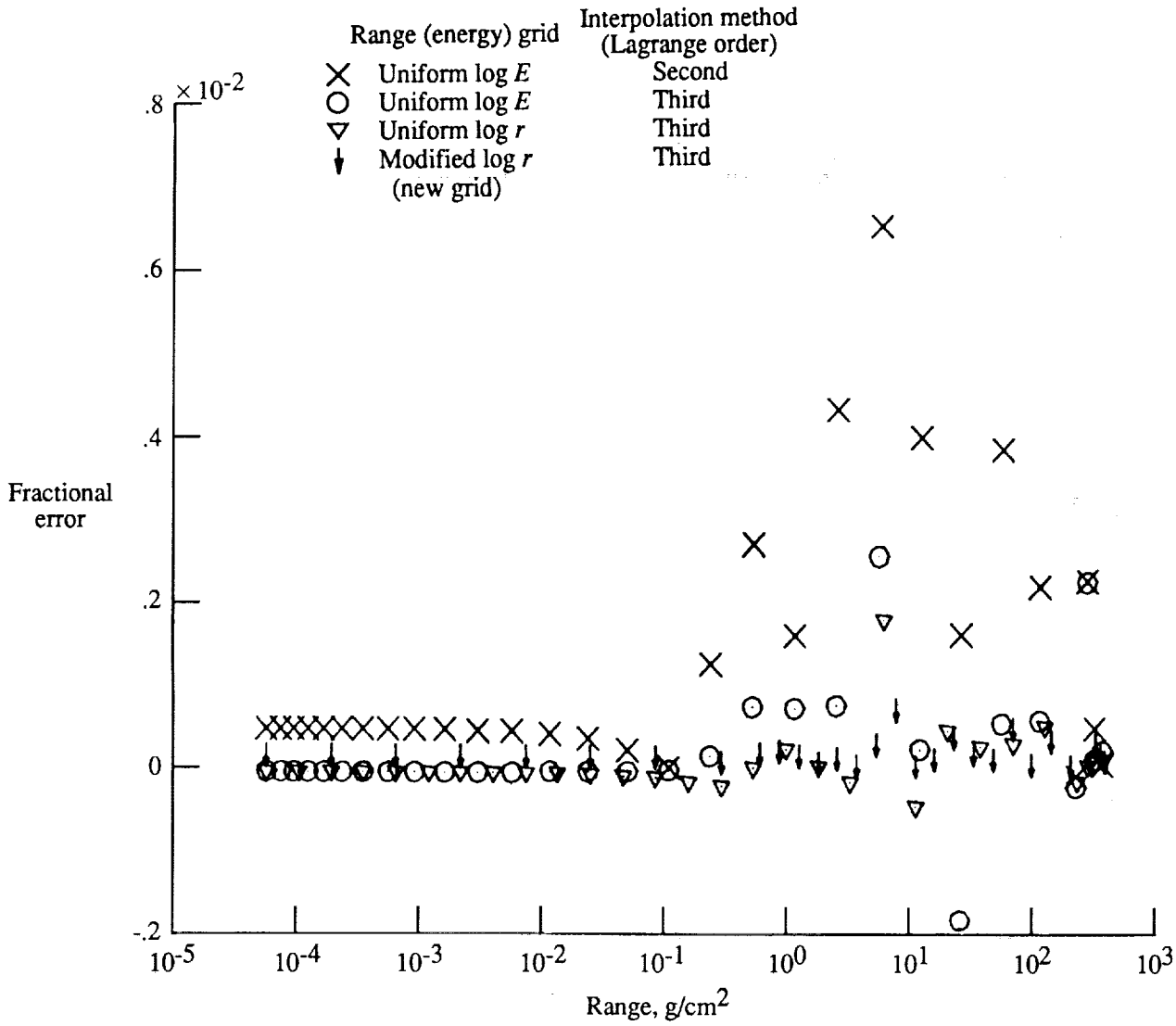

(b) $h = 1$ g/cm^2.

Figure 5. Concluded.

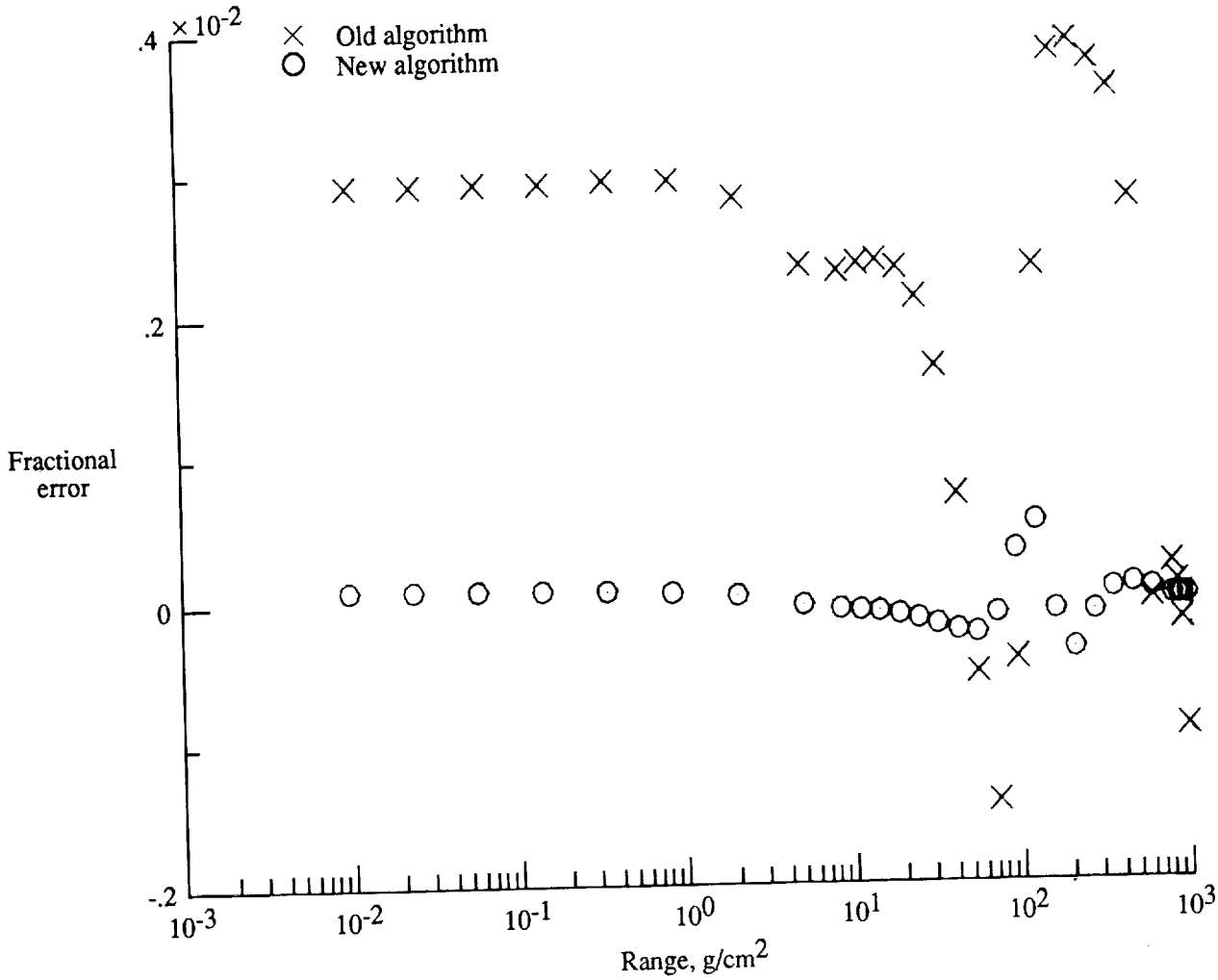

Figure 6. Fractional error of integrating the February 1956 SPE spectrum using existing and new algorithms.

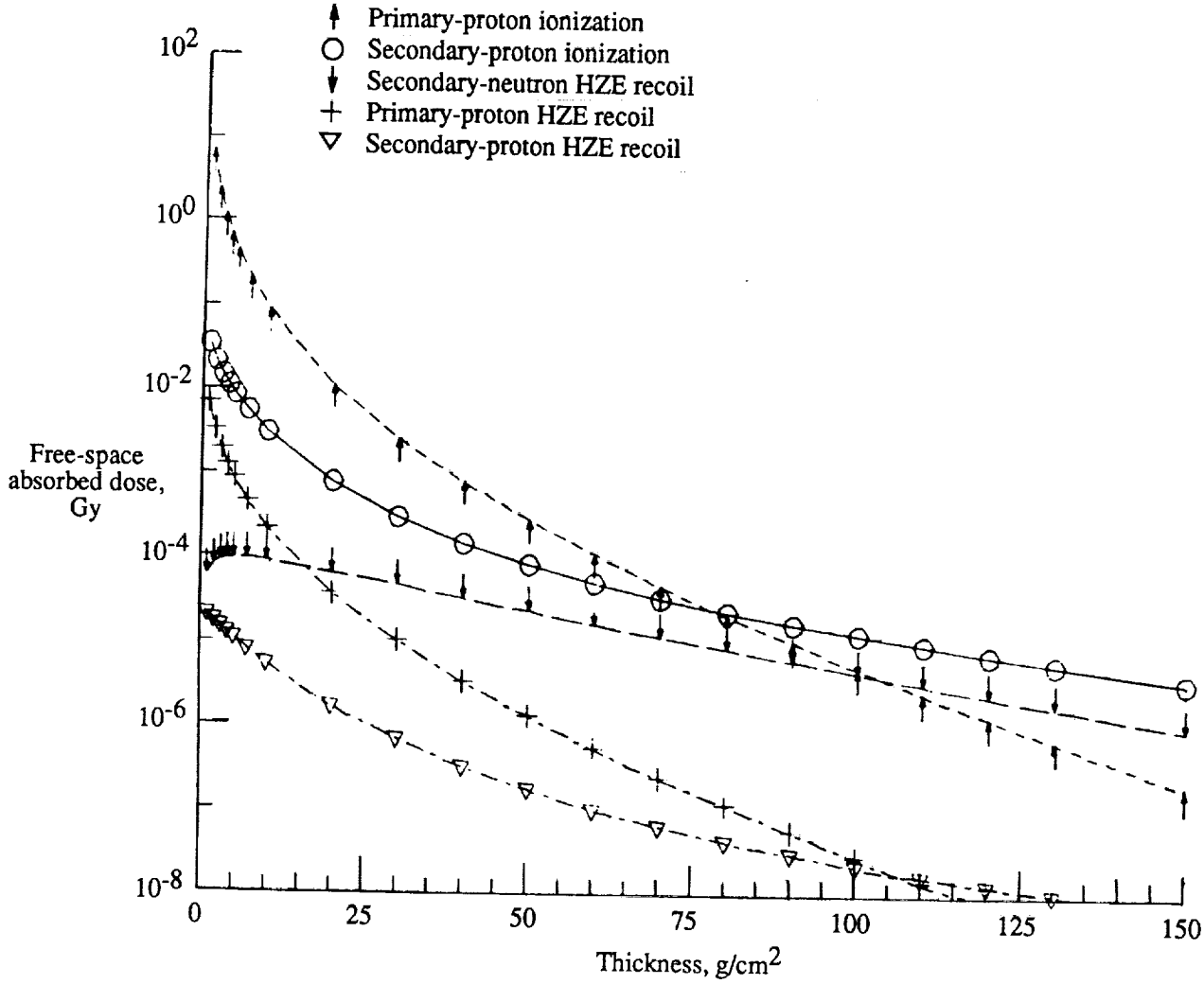

(a) $N = 30$.

Figure 7. Free-space absorbed doses to the August 1989 SPE spectrum as a function of aluminum thickness. New algorithms.

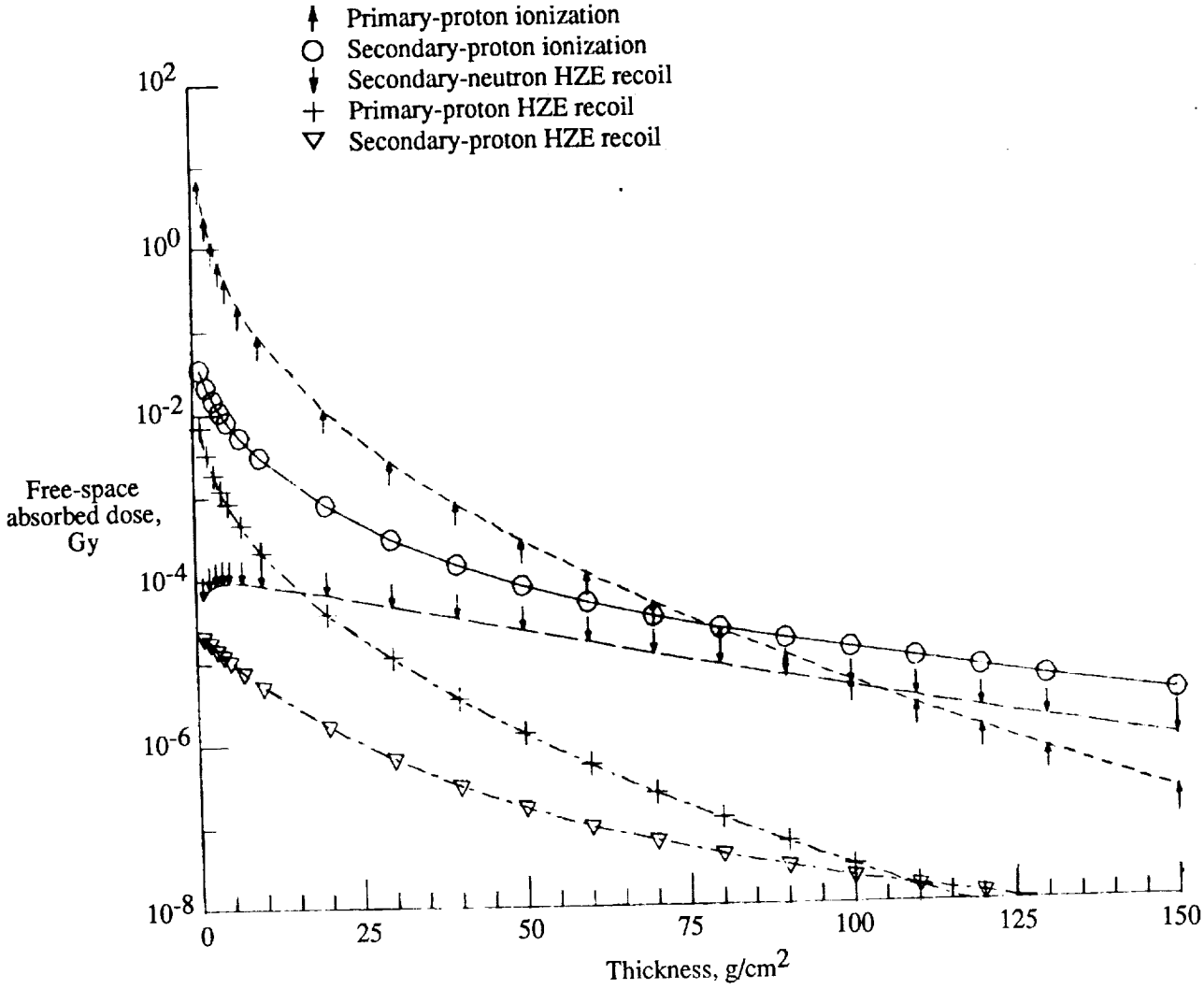

(b) $N = 60$.

Figure 7. Continued.

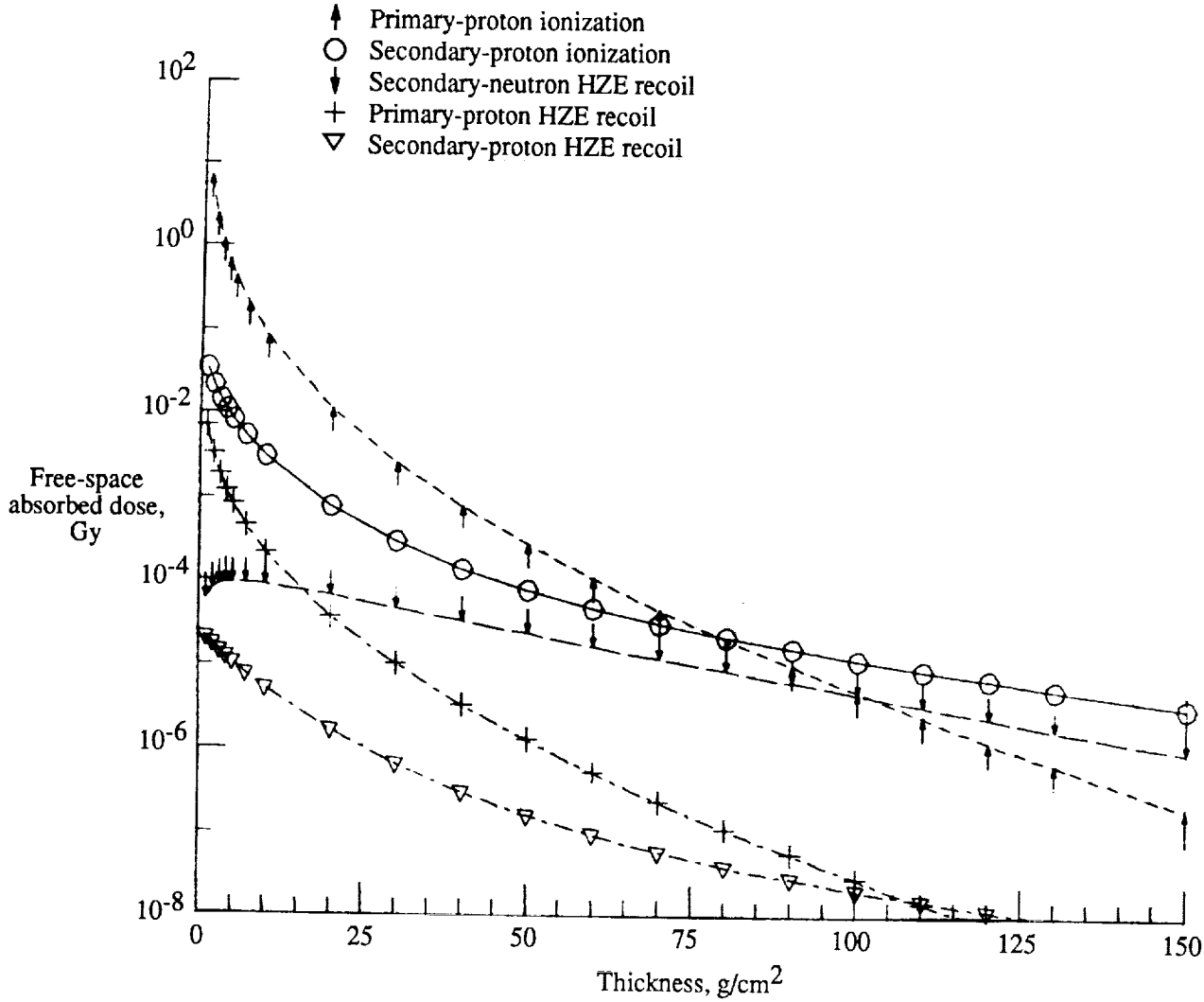

(c) $N = 90$.

Figure 7. Concluded.

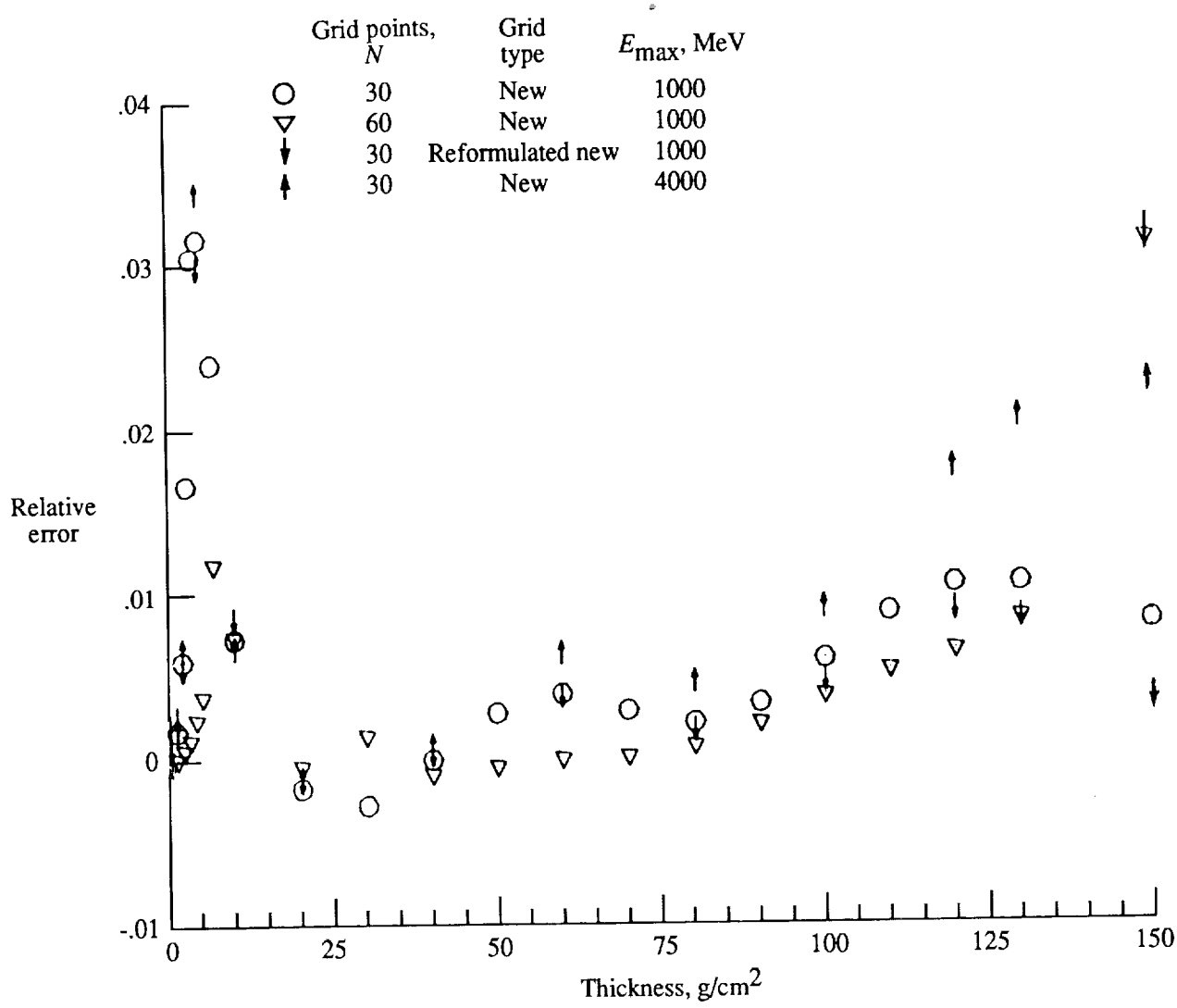

(a) Primary-proton ionization dose.

Figure 8. Relative errors in doses to those calculated with 90 grid points. Doses are the same as those in figure 7.

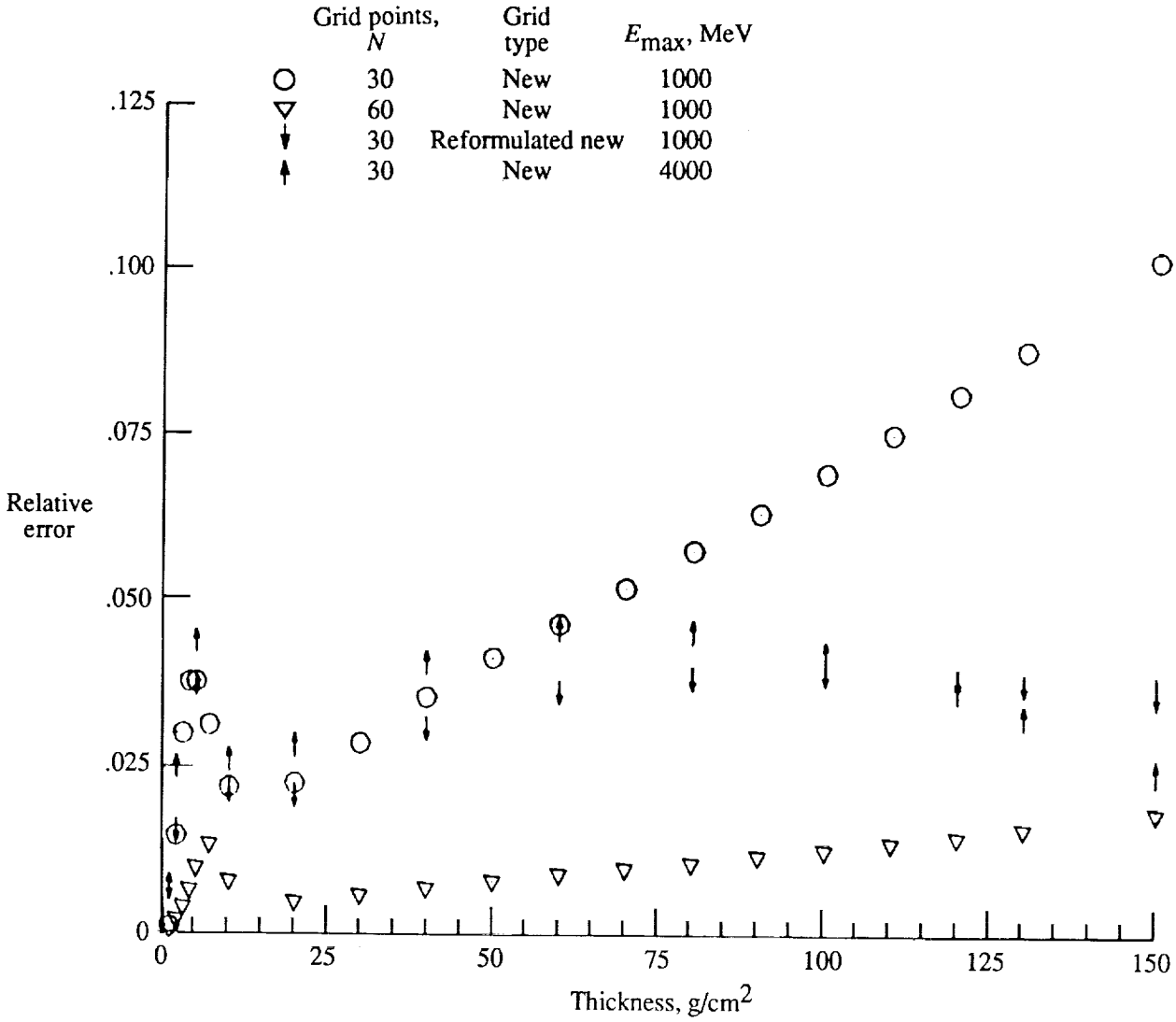

(b) Secondary-proton ionization dose.

Figure 8. Continued.

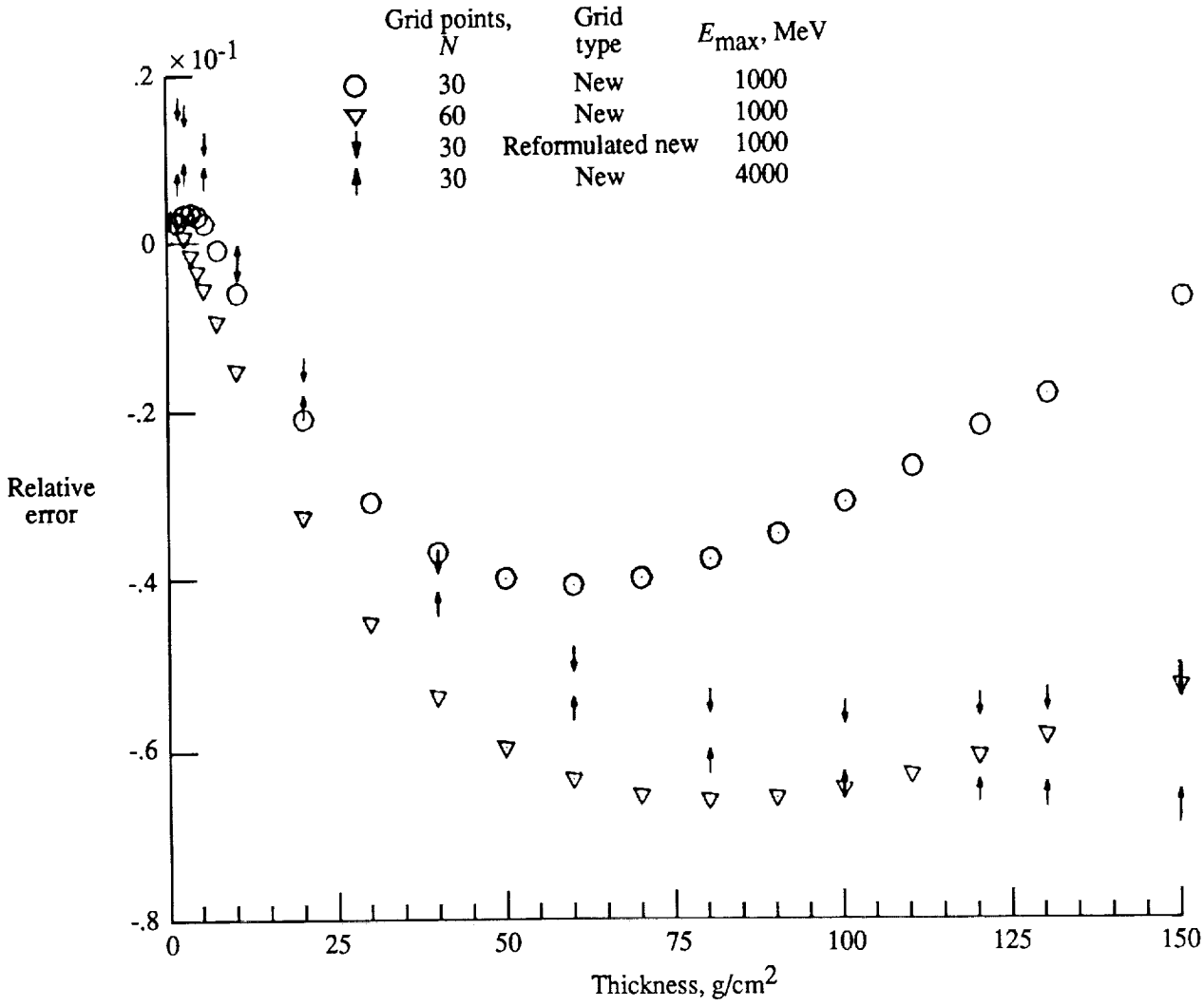

(c) Secondary-neutron HZE recoil dose.

Figure 8. Concluded.

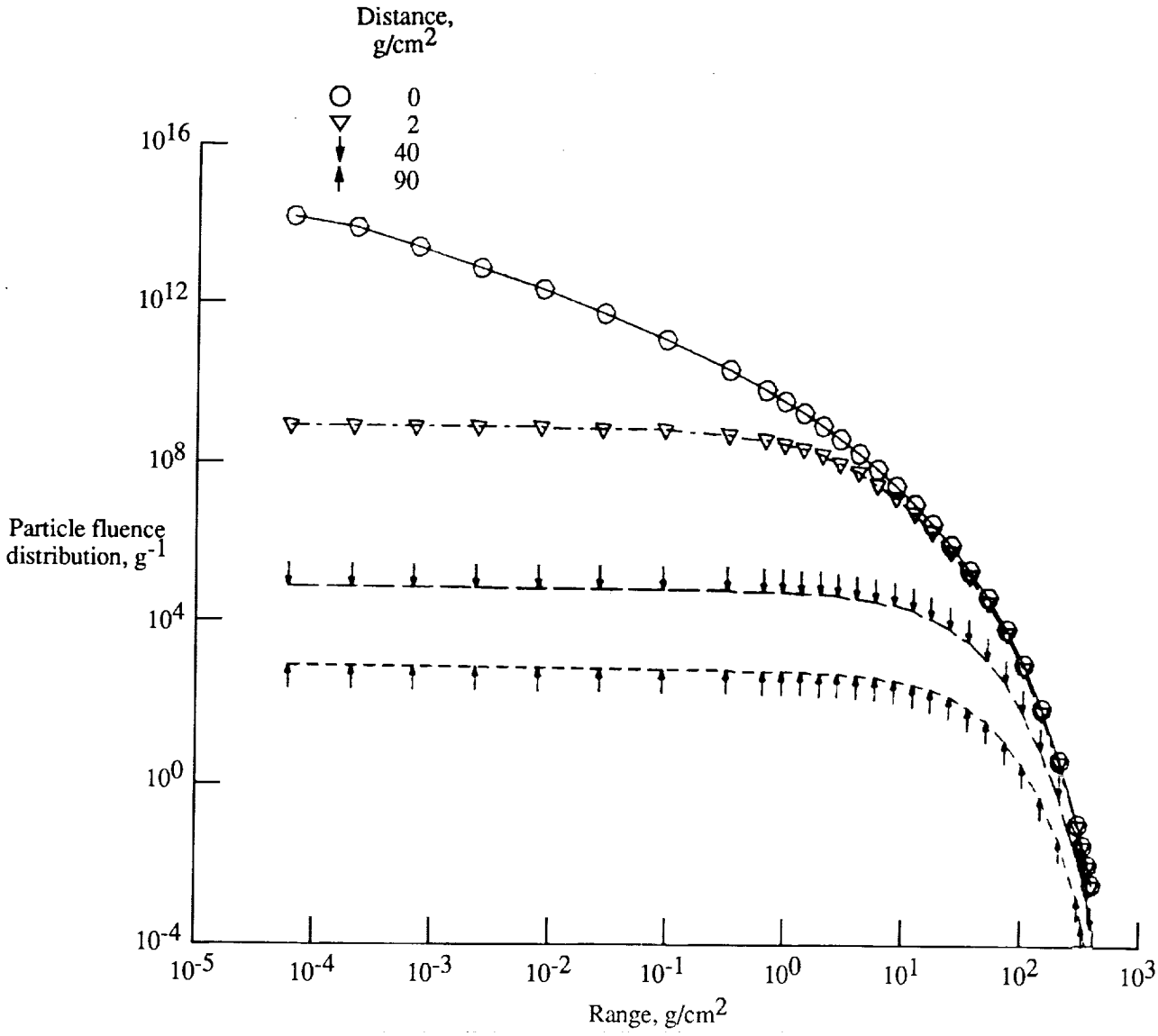

(a) Primary protons.

Figure 9. Distribution of various field components (in transformed coordinates) in aluminum shield at distances from boundary exposed to the August 1989 SPE spectrum. New algorithms.

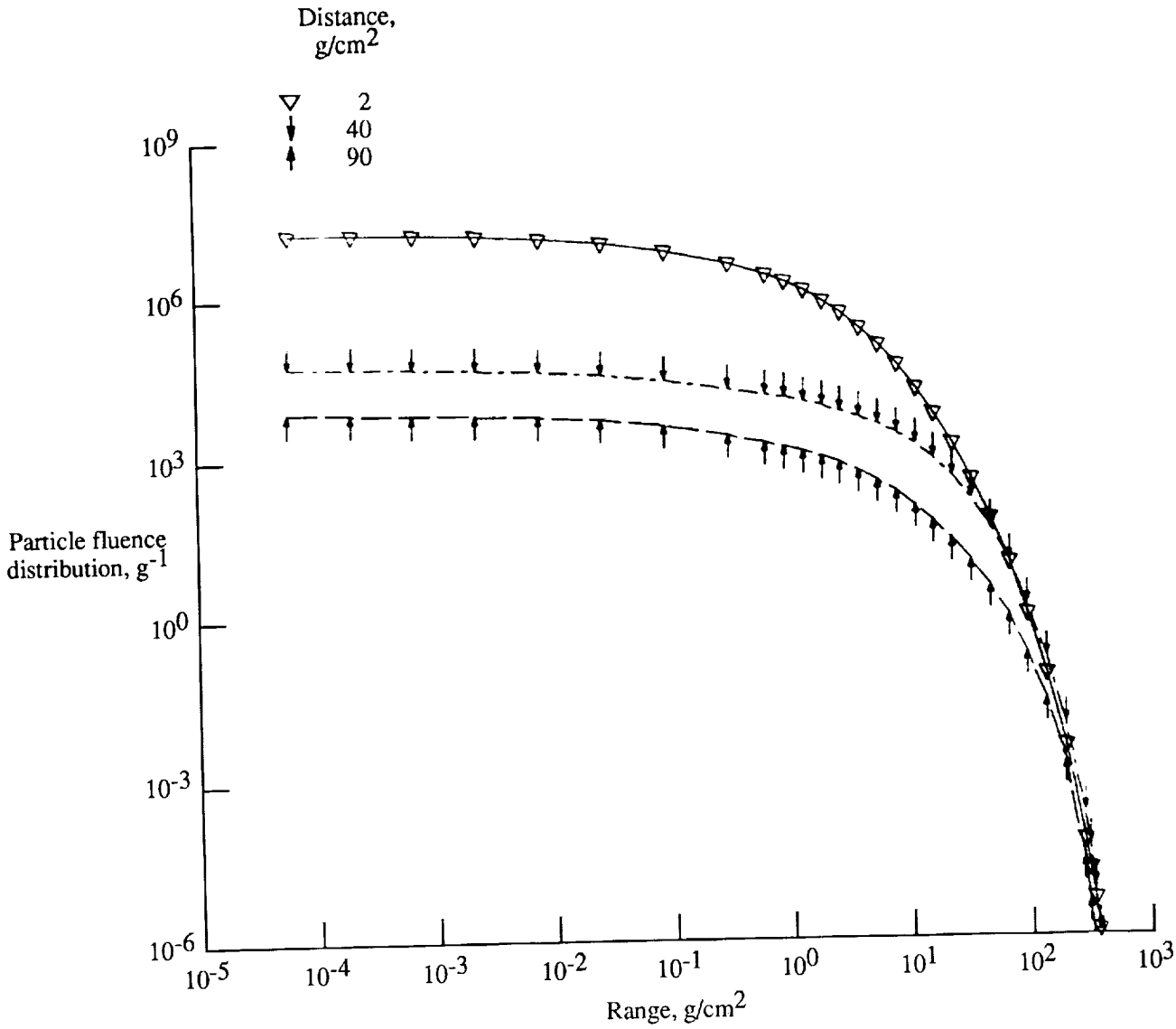

(b) Secondary protons.

Figure 9. Continued.

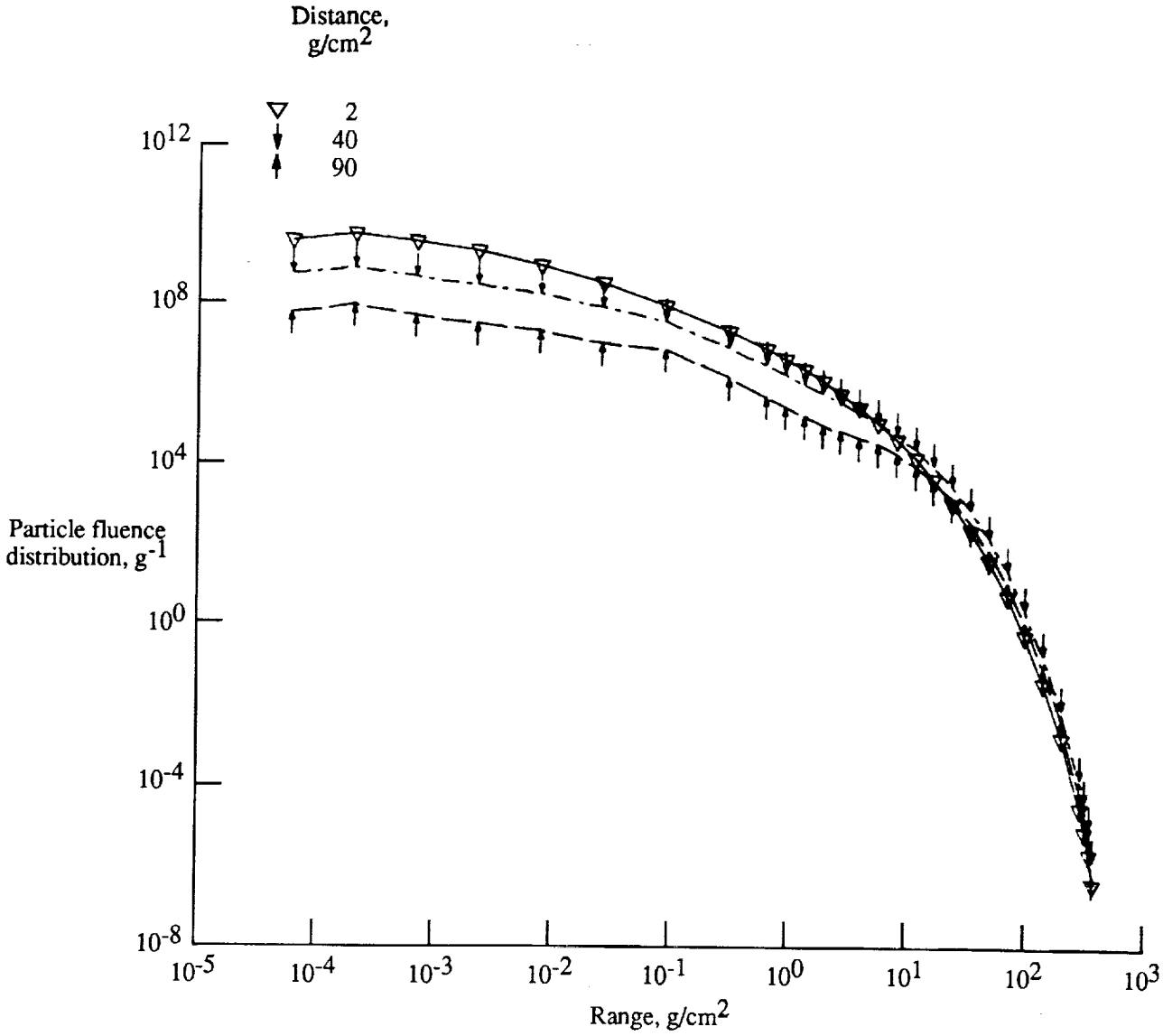

(c) Secondary neutrons.

Figure 9. Concluded.

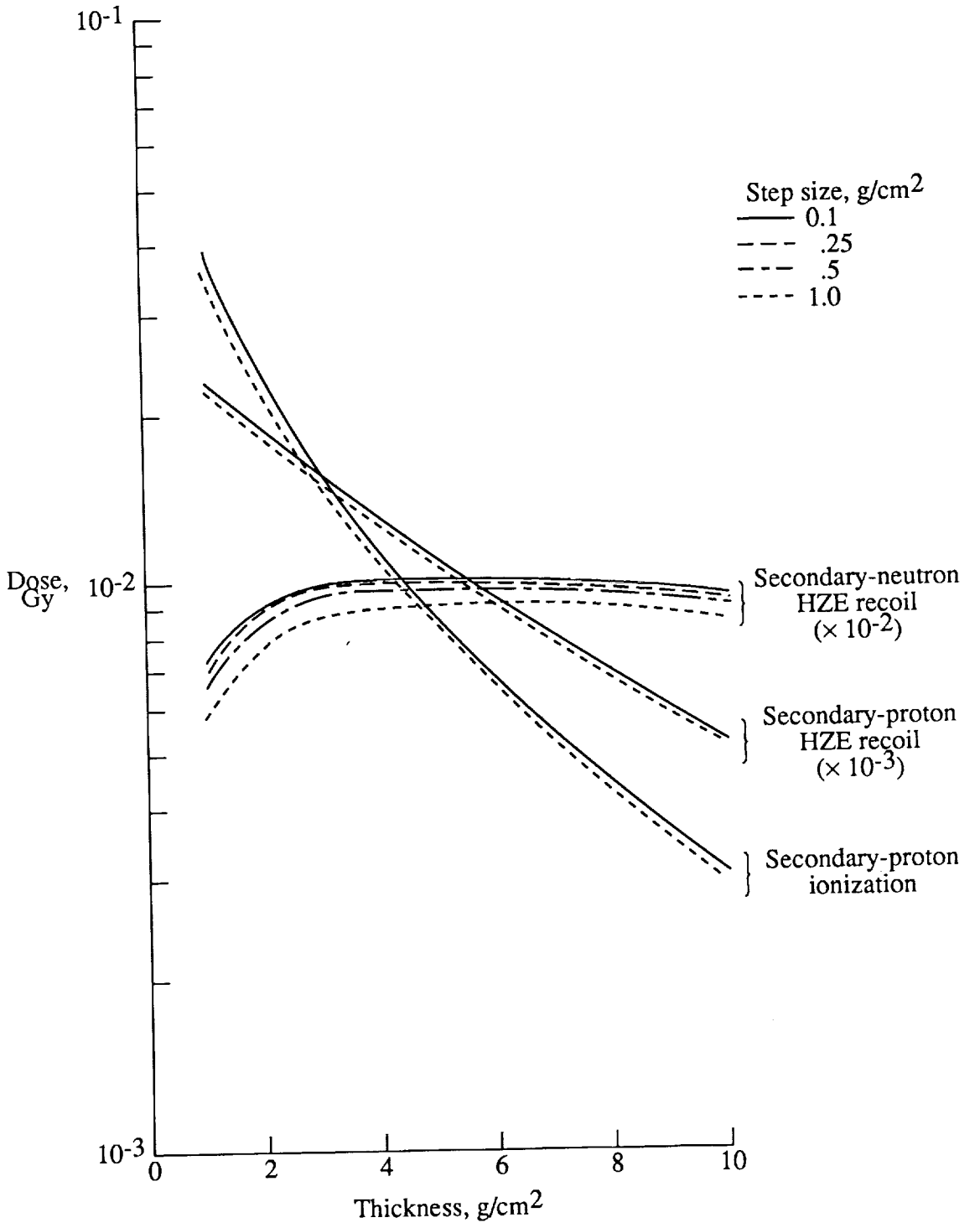

Figure 10. Free-space absorbed secondary doses to the August 1989 SPE spectrum as a function of aluminum thickness. New algorithms with varying step size.

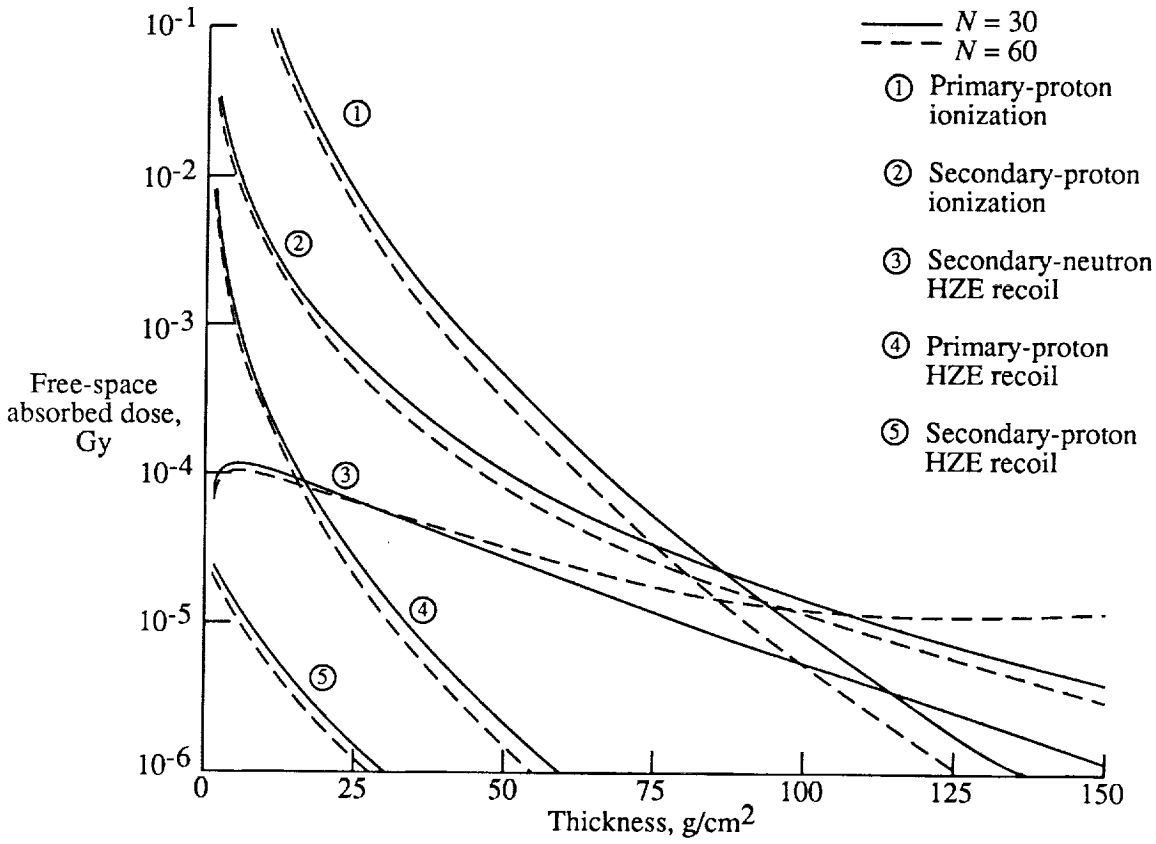

Figure 11. Free-space absorbed doses to the August 1989 SPE spectrum as a function of aluminum thickness. Old BRYNTRN algorithms.

NASA
National Aeronautics and Space Administration

Report Documentation Page

1. Report No.	2. Government Accession No.	3. Recipient's Catalog No.
NASA TP-3093		

4. Title and Subtitle	5. Report Date
Improvements in Computational Accuracy of BRYNTRN (A Baryon Transport Code)	May 1991
	6. Performing Organization Code
7. Author(s)	8. Performing Organization Report No.
Judy L. Shinn, John W. Wilson, Mark Weyland, and Francis A. Cucinotta	L-16898
9. Performing Organization Name and Address	10. Work Unit No.
NASA Langley Research Center Hampton, VA 23665-5225	199-04-16-11
	11. Contract or Grant No.
12. Sponsoring Agency Name and Address	13. Type of Report and Period Covered
National Aeronautics and Space Administration Washington, DC 20546-0001	Technical Paper
	14. Sponsoring Agency Code

15. Supplementary Notes

Judy L. Shinn and John W. Wilson: Langley Research Center, Hampton, Virginia.
Mark Weyland: Kelsey-Seybold Clinic, Lyndon B. Johnson Space Center, Houston, Texas.
Francis A. Cucinotta: Rockwell International, Houston, Texas, now at Langley Research Center, Hampton, Virginia.

16. Abstract

The extension of the baryon transport code (BRYNTRN) for use in space radiation dose analyses for very large shield thicknesses is made possible by improving the numerical algorithms. The efforts were concentrated in obtaining more accurate, yet efficient, interpolation and integration methods at each local computational step, and in optimizing the grid distributions. A brief discussion of the nucleon transport theory and propagating formula is also given in conjunction with the analysis of error propagation which reveals the need for minimizing the local truncation errors. Sample calculations were made to verify the new algorithms. An accuracy of approximately 5 percent for a shield thickness of 150 g/cm^2 was found when a minimal 30-point energy grid was used. This accuracy was far superior to the results obtained by using the old algorithms where the solutions could be an order of magnitude different when a reasonably large number of grid points were used. The propagating step size was chosen such that the perturbation theory error matched the improved numerical accuracy.

17. Key Words (Suggested by Author(s))

Space radiation
Numerical accuracy
High-energy transport

18. Distribution Statement

Unclassified—Unlimited

Subject Category 93

19. Security Classif. (of this report)	20. Security Classif. (of this page)	21. No. of Pages	22. Price
Unclassified	Unclassified	35	A03

For sale by the National Technical Information Service, Springfield, Virginia 22161-2171